NTNU – Trondheim
Norwegian University of
Science and Technology

Non-invasive Ultrasonic Inspection Through Steel Pipes Using the SURF Method

Håkon Haugenes Rake

Electronics System Design and Innovation
Submission date: June 2014
Supervisor: Odd Kr. Pettersen, IET
Co-supervisor: Tonni Franke Johansen, SINTEF

Norwegian University of Science and Technology
Department of Electronics and Telecommunications

Problem Description

Non-invasive Ultrasonic Inspection Through Steel Pipes Using the SURF Method

Study the possibility of establishing a simulation tool for the so-called SURF method for acoustic wave propagation through steel pipes using finite element modeling and COMSOL. The goal is to establish a simplified SURF modeling scheme of non-linear wave propagation as expressed by the SURF method, i.e. two waves are transmitted simultaneously in the same direction with a large frequency ratio of about 1:10. The method should be tested with waves at normal and oblique incident against a steel pipe.

Ultralydinspeksjon gjennom stålrør ved hjelp av SURF-metoden

Det skal undersøkes hvorvidt en kan etablere et simuleringsverktøy for den såkalte SURF-metoden for akustisk bølgeforplanting gjennom stål ved hjelp av elementmetoden og COMSOL. Målsetningen er å etablere et forenklet modelleringsskjema av ikke-lineær bølgeforplantning slik det framkommer med SURF-metoden, dvs. at det sendes bølger ved to frekvenser med stor avstand i frekvens, typisk forholdstall 1:10. Metoden skal testes ved bølger ved normalt innfall og skrått innfall mot stålrør.

Summary

The main objective of this thesis has been to study the possibility to establish a simulation tool for *Second Order Ultrasonic Field* (SURF) based on finite element modeling implemented in COMSOL Multiphysics. The SURF method is a dual-frequency ultrasonic imaging technique where two waves are transmitted in the same direction with a large separation in frequency of about 1:10. This causes interaction between the waves, which give rise to non-linear sound propagation. The method can be used for enhanced ultrasonic imaging capabilities. The COMSOL implementation has been documented and through studies of normal incident waves and oblique incident waves at a steel interface, the advantages and disadvantages of the implementation has been highlighted.

The SURF method has been implemented in the built-in physical interfaces of *Pressure Acoustics* and *Acoustic-Solid Interaction* in COMSOL. Simple 2D normal incident plane wave simulations have been compared to theoretically calculated values of non-linear speed of sound, with matching results. The study of the plane wave model has been extended to include water and steel modeled as both linear and non-linear materials. Studies on the possibility of analyzing non-linear materials behind steel have shown possible ways to ensure transmission through steel, despite high impedance ratios between water and steel. The most promising methods proved to be based on impedance matching and standing waves which coincides with other studies on the topic.

Simulations with the *Acoustic-Solid Interaction* interface on large models, which include structural waves and deformations, have been bounded to a low frequency study in a SURF scheme. This is because of a rapidly increasing computational time, as a function of degrees of freedom to solve for in the model. Estimations predict solution time of in terms of weeks on large scale models, when the fundamental convergence criteria of elements per wavelength and number time steps in a time dependent finite element analysis are fulfilled. Possible measures to overcome this are performing the simulations on a more powerful computer, modifying the implemented solution process or using a different solver than the direct solver used in this thesis.

Sammendrag

Hovedmålet med denne oppgaven har vært å studere mulighetene for å etablere et simuleringsverktøy for SURF-metoden basert på modellering med elementmetoden implementert i COMSOL Multiphysics. SURF-metoden er en to-frekvens ultralydavbildningsteknikk, hvor to bølger blir transmittert i samme retning med en stor forskjell i frekvens på omtrent 1:10. Dette fører til interaksjon mellom bølgene, som resulterer i ikke-lineær bølgeforplantning som kan benyttes til forbedret ultralydavbildning. Implementeringen i COMSOL har blitt dokumentert, og gjennom studier av normalt og skrått innfallende bølger mot en grenseflate av stål har fordeler og ulemper ved implementering blitt trukket fram.

SURF-metoden har blitt implementert i de innebygde fysikkgrensesnittene 'Pressure Acoustics' og 'Acousti-Solid Interaction' i COMSOL. Enkle 2D-planbølgesimuleringer av normalt innfallende bølger har blitt sammenlignet med teoretisk beregnede verdier for den ikke-lineære lydpropagasjonen, og disse viste god overensstemmelse. Studien av planbølger er utvidet til å inkludere vann og stål, både lineært og ikke-lineært. Studier av muligheten til å analysere ikke-lineære materialer bak stål har vist mulige måter for å få transmisjon gjennom stål, til tross for den store impedansforskjellen mellom stål og vann. De mest lovende metodene viste seg å være basert på impedanstilpasning og stående bølger. Dette sammenfaller med tidligere studier av temaet.

Simuleringen med brukergrensesnittet 'Acoustic-solid interaction' på modeller med store dimensjoner, som inkluderer strukturelle bølger og deformasjoner, har blitt begrenset til en lavfrekvensstudie i en SURF-analyse. Årsaken til dette er raskt økende beregningstid som funksjon av antallet frihetsgrader å løse i modellen. Estimeringer predikerer en beregningstid på flere uker, når de fundamentale konvergenskriteriene om elementer per bølgelengde og antall tidstrinn i en tidsavhenging studie med elementmetoden er tilfredsstilte. Mulige tiltak for å minske beregningstiden kan være å anvende mer beregningskraft, modifisere den implementerte løsningsprosessen eller bruk av en annen løser enn den direkte løseren anvendt i denne oppgaven.

Preface

The work in this thesis is the concluding part of my M.Sc degree at the Department of Electronics and Telecommunication at the Norwegian University of Science and Technology (NTNU). The topic of the thesis was presented by Professor Odd K. Pettersen at SINTEF. The thesis was written in the period between January and June 2014.

Firstly, I would like to thank my supervisor Tonni Franke Johansen at SINTEF for the inspiring discussions on the topic of ultrasonics, guiding me in the right direction, and most of all taking the time to get involved in this thesis. I would also like to show my gratitude for the technical help provided by COMSOL on advanced modeling topics.

Håkon Haugenes Rake, June 2014, Trondheim.

Contents

List of Figures

List of Tables

List of Abbreviations

TOF	Time Of Flight
HF	High Frequency
LF	Low Frequency
SURF	Second order UltRasound Field
FE	Finite Element
FEM	Finite Element Method
FEA	Finite Element Analysis
NLL	Non-Linear Layer
BC	Boundary Condition
NDE	Non Destructive Evaluation
SW	Standing Waves
PML	Perfectly Matched Layer
NLM	Non-Linear Medium
PDE	Partial Differential Equation
CAD	Computer-Aided Design
CFL	Courant-Friedrichs-Lewy
EPW	Elements Per Wave Length
NTNU	Norwegian University of Science and Technology

1 | Introduction

1.1 Background and Motivation

Ultrasound is the general name of oscillating pressure waves with a frequency greater than the human threshold of hearing, i.e. above 20 KHz. The applications using ultrasound today are numerous, stretching from sound navigation and ranging (SONAR) to non-invasive medical imaging and non-destructive testing (NDT). Using ultrasound for NDT to detect internal flaws and characterization of materials is a well-established approach. Common examples of NDT with ultrasound are wall thickness measurements and detecting flaws in steel welds and pipes. Ultrasonic testing offers many advantages over invasive techniques, such as safety, efficiency, no system shut down and the possibility of remote monitoring.

One of the most commonly known applications of ultrasound is within medical imaging and diagnostics. The technology has evolved from low resolution 2D images to high resolution 3D images by utilizing increasing computational power, new transducer designs and the development of improved signal processing methods. An example of this is harmonic imaging, which exploit the non-linear properties of sound propagation, improving both accuracy and the resolution of the images [1]. One method which evolved from harmonic ultrasound imaging is the Second Order Ultrasound Field method (SURF). In SURF imaging a dual-frequency technique is utilized, where two pulses are transmitted simultaneously in the same direction with a large frequency ratio of about 1:10. The low frequency (LF) pulse modifies the elastic property of the medium observed by the high frequency (HF) pulse [2]. The modulation of the material properties, give rise to non-linear propagation effects of the HF pulse, leading to improved diagnostic capabilities. The method has proved strong potential within acoustic noise suppression, contrast agent detection and micro calcification detection [3].

A possible application of the SURF method beyond medical imaging is non-destructive testing of materials. The possibility has been investigated in a non-invasive ultrasound inspection through steel scheme as described in [4]. This is a part of the SmartPipe project, aimed at developing a concept for NDT and remote monitoring of steel pipes [4]. The concept is highly attractive for the petroleum industry as it benefits of all the advantages of NDT, including reliability and cost effectiveness.

1.2 Purpose of This Study

The subject of this study is to examine the possibility to establish a simulation tool for the SURF method for acoustic waves through steel pipes using finite element modeling (FEM) with COMSOL Multiphysics. The goal is to have a simplified FEM model of the non-linear propagation described by SURF. This is very desirable, since FEM modeling can be a highly effective and versatile method to examine propagation in different mediums and geometries. However, implementing the SURF effect into COMSOL is not a trivial task, since it is necessary to modify the governing equation and couple a high frequency and low frequency solution. Another challenge is the computational complexity due to the high frequencies involved, because it is necessary to have at least six finite elements per wave length to ensure convergence in the solution. The SURF model in COMSOL is to be implemented in a fluid and a structural physical interface. The model has to be properly verified, to ensure no unwanted effects in the computation. The simulations will be made on both normal and oblique incident waves on a steel layer.

1.3 Outline of Thesis

The outline of the thesis is as follows. In Chapter 2 relevant theory is presented. It starts with an introduction to wave propagation, both linear and non-linear, to be able of understanding the SURF method, before the core principles of sound transmission and ultrasonic imaging is discussed. The chapter ends with an explanation of the fundamentals of finite element modeling.

Chapter 3 is dedicated to present the equipment. The core equipment in this thesis is COMSOL, which is presented further in depth. The main functionality and processing scheme is first presented, before relevant physical interfaces are presented more thoroughly.

Chapter 4 presents the modifications made in COMSOL to the governing equation in detail, followed by descriptions of the simulated models, with arguments on the choice of geometry, physics, source modeling and computational factors. In Chapter 5 the simulations results are presented and discussed considering generality and validity. Chapter 6 includes a final conclusion with remarks on further work.

2 | Theory

2.1 Acoustic Waves

The acoustic wave equation describes the propagation of acoustic waves in a medium. This is essentially a second order differential equation describing the evolution of pressure as a function of position and time. Governed by the assumptions in the derivation, it can be regarded as linear or non-linear. In this thesis both subjects are covered to be able to describe the difference between linear and non-linear acoustics, it is essential to give a brief description of both theories. A more detailed description is found in [5] and [6].

2.1.1 Linear Wave Equation

In a medium where a wave propagates there will be a local change in density generated by the wave's displacement in the medium. This causes a formation of forces that act to restore the density of the medium to the equilibrium state. Describing acoustic waves in fluids, the wave equation can be developed with foundation in the laws of mass, momentum and energy conservation:

- The conservation of mass:

$$\frac{\partial \rho}{\partial t} = -\nabla \cdot (\rho \boldsymbol{v}) \tag{2.1}$$

- Eulers equations, describing the momentum balance:

$$\rho \left[\frac{\partial \boldsymbol{v}}{\partial t} + \boldsymbol{v} \cdot \nabla \boldsymbol{v} \right] = -\nabla p \tag{2.2}$$

- The equation of state giving the relationship between change in density and pressure assuming constant entropy:

$$p = p(\rho) \tag{2.3}$$

where ρ is the density , p is the pressure and $\boldsymbol{v}$ is the particle velocity. These three equations are non-linear by nature. By using a combination of these equations and the process of linearization, one ends up with the classical linear acoustic theory. The details are described in [5]. The main step in this process is using only first order terms in the expansion of the governing non-linear

equations. Another assumption is that amplitudes are small. This leads to classic linear, lossless wave equation describing the propagation of sound in fluids:

$$\nabla^2 p - \frac{1}{c_0^2}\frac{\partial^2 p}{\partial t^2} = 0 \tag{2.4}$$

In this equation p is the pressure and c_0 is the speed of sound, defined as:

$$c_0 = \sqrt{\frac{K_0}{\rho_0}} \tag{2.5}$$

The value of the bulk modulus K_0 and the density ρ_0 is dependent on the properties of the medium, so conditions such as temperature and pressure may change the value of the speed of sound c_0.

2.1.2 Non-linear Wave Equation

When deriving the linear acoustic wave equation, it is assumed small amplitudes and a linear relationship in the governing equations given by equation (2.1),(2.2) and (2.3) leading to drop high order terms, which in some situations is a considerable simplification. Following the discussion in [7], expansion of the equation of state in equation (2.3) as a taylor series, including the first two terms:

$$p = p_0 + A(\frac{\rho - \rho_0}{\rho_0}) + \frac{B}{2}(\frac{\rho - \rho_0}{\rho_0})^2 ... \tag{2.6}$$

where the coefficients of the expansion are:

$$A = \rho_0(\frac{\partial p}{\partial \rho})_0,\ B = \rho_0^2(\frac{\partial^2 p}{\partial \rho^2})_0 \tag{2.7}$$

where the subscript 0 indicates equilibrium. The higher order terms in this series describes the non-linear effect. In the linear case with infinitely small amplitudes the speed of sound is simply described as in equation (2.5), since A is identical to the bulk modulus K_0.

The wave equation that account for non-linearity of second order defined by (2.6), is the Westervelt equation:

$$\nabla^2 p - \frac{1}{c_0^2}\frac{\partial^2 p}{\partial t^2} + \frac{\delta}{c_0^4}\frac{\partial^3 p}{\partial t^3} = -\frac{\beta}{\rho_0 c_0^4}\frac{\partial^2 p^2}{\partial t^2} \tag{2.8}$$

where δ is the sound diffusivity and β is the non-linear parameter. To describe the degree of non-linearity in a material customary to use the two non-linear parameters B/A and β introduced in the Westervelt equation, which describe the degree of non-linear effects in different materials:

$$\frac{B}{A} = \frac{\rho_0}{c_0^2}(\frac{\partial^2 p}{\partial \rho^2})_0 \tag{2.9}$$

and

$$\beta = (1 + \frac{B}{2A}) \tag{2.10}$$

The second non-linear effect derives from the equation of conservation of mass. By algebraic manipulation and further assumptions described in [8], one end with a modified expression for the non-linear speed of sound:

$$c = c_0(1 + \beta M) = c_0(1 + \beta \kappa p) \tag{2.11}$$

where M is the Mach number. Equation (2.11) describes how the non-linear propagation velocity varies with volume compression of the material. As the wave propagates it will progressively get distorted, since the speed of sound varies with the pressure amplitude. The higher amplitude implies locally increased wave speed and lower amplitude the opposite. Figure 2.1 illustrates how a high pressure amplitude wave gradually has been distorted due to the non-linear non-linear effects, as described by (2.8) and observed in [1]. Even though it seems that the effect is ever increasing, this is not the case. The distortion generates high frequency harmonics which is rapidly attenuated due to frequency dependent absorption.

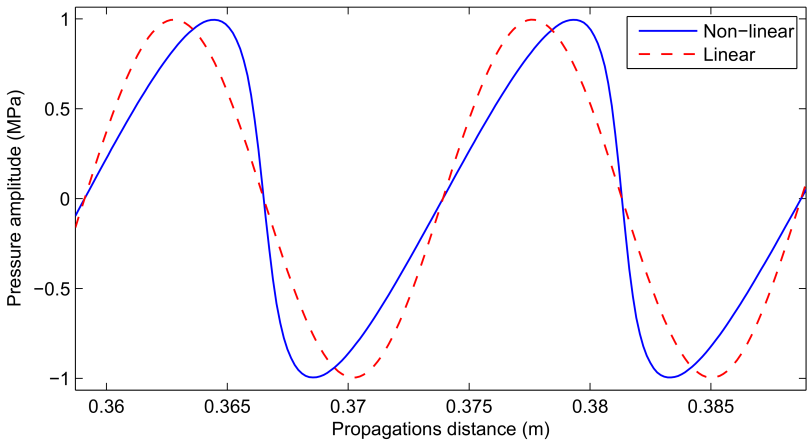

Figure 2.1: Linear propagation and non-linear propagation with distortion [1]

2.1.3 Transmission of Sound Waves

In general acoustics and in diagnostic ultrasound it is important to model the transmission of sound waves through mediums with different acoustic properties. This is a vast topic and will in this theory be simplified to normal incident and oblique incident waves in a fluid medium. This means that solid materials with structural waves are omitted in this discussion, for some application this can be a significant simplification.

The simplest case is when a normal incident planar wave hits a boundary between two fluid medium. These media can be described acoustically in terms

of the density ρ and the speed of sound c. Using the material parameters, the transmission can be described by using the boundary condition of continuity of pressure and particle velocities at the interface. By considering the intensities of the incoming, the reflected and the transmitted wave it can be shown that reflection R_P and transmission T_p coefficients at the interface between two media are:

$$R_p = \frac{Z_2 - Z_1}{Z_2 + Z_1} \tag{2.12}$$

$$T_p = \frac{2Z_2}{Z_2 + Z_1} \tag{2.13}$$

where $Z_n = \rho_n c_n$ is the the acoustic impedance of medium 1 and 2. The equations fully describe the transfer of energy in the transmission. By proceeding the discussion it is possible to view the structure as an acoustic delay line, where each element (interface) have an impedance Z_n, wavenumber κ_n and length l_n in such a way that the boundary conditions are satisfied. The input impedance Z_in of a line terminated by the impedance Z_2 is then:

$$Z_{in} = Z_0 \frac{Z_2 - iZ_0\, tan(\kappa l)}{Z_0 - iZ_0\, tan(\kappa l)} \tag{2.14}$$

Examining equation (2.14) gives two special cases of special interest. If a wave of a certain frequency f hits the interface and the interface has a matching length of $\lambda/2$ in reference to the waves wave length in the propagation medium, the term of $tan(\kappa l)$ is zero. This leads to an input impedance of:

$$Z_{in} = Z_2 \tag{2.15}$$

The input impedance is transferred without change, the interface is invisible to the incoming wave and it is possible to have full transmission without loss, because of resonance. The physical basis for the resonance is that the waves reflected internally in the plate are in phase with the original wave creating a standing wave pattern (SW). It may be necessary that the pulse is several wavelengths long to build up SW and thereby resonance in the middle layer. The other case is when the interface has a length of $\lambda/4$. With a middle layer of length $\lambda/4$ the term of $tan(\kappa l)$ in equation (2.14) is infinite, resulting in a input impedance of:

$$Z_{in} = \frac{Z_0^2}{Z_2} \tag{2.16}$$

This is a quarter-wavelength impedance transformer, which has the possibility to transform a load impedance Z_2 into an input impedance Z_{in}. The transmission and reflection coefficient for the case of a three layer structure ended with an infinite half space is derived by the same discussion for oblique incident angle, as described in [8]. The reflection coefficient is given by:

$$R_0 = \frac{r_{01} + r_{12}e^{(2i\gamma_1 l_1)}}{1 + r_{01}r_{12}e^{(2i\gamma_1 l_1)}} \tag{2.17}$$

where θ is the incident angle, l_1 it the layer thickness, r_{nm} is the reflection coefficient between layer n and m and γ_n is the vertical wave number of the incident wave, defined as:

$$\gamma_n = \frac{\omega}{c_n} \sin(\theta_n) \tag{2.18}$$

The transmission coefficient is given by the identical parameters as:

$$T_2 = \frac{t_{01} + t_{12} e^{(2i\gamma_1 l_1)}}{1 + t_{01} t_{12} e^{(i\gamma_1 l_1)}} \tag{2.19}$$

To illustrate the transmission and reflection coefficient, consider a 2 cm thick plate with density $\rho = 7500$ kg/m^3 and speed of sound $c = 5000$ m/s placed between two infinite layers of water with density $\rho = 1000$ kg/m^3 and speed of sound $c = 1500$ m/s. The example is inspired by the discussion on the topic in [8]. The reflection and transmission coefficient for this case is illustrated in figure 2.2, as a function of frequency with incident angle $\theta = 0$ using equation (2.17) and (2.19). In the figure a periodic pattern of high transmission can be spotted, with periodicity of a half wavelength matched to the thickness. Due to large difference in impedance between the materials there are almost no transmission unless the thickness of the middle layer is an integer number of half a wavelength in the middle layer as stated by equation (2.15). The reflection coefficient is plotted to verify the conservation of energy and is as expected the inverse of the transmission coefficient.

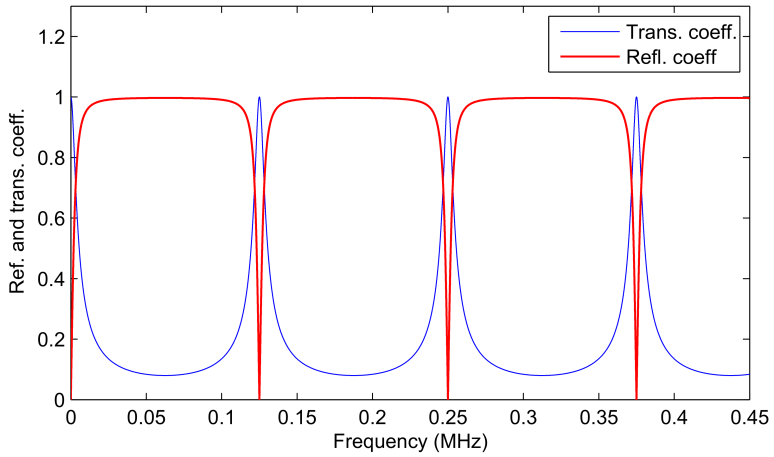

Figure 2.2: Reflection and transmission coefficient through a layer with thickness l bounded by to semi-infinite medium

2.1.4 Ultrasonic Pulse-echo Imaging

There are mainly two main methods of ultrasonic imaging, which is *pitch-catch* and *pulse-echo*. The *pulse-echo* method is the generally most widely used method, where the source and receiver is the same transducer. This is the standard method for generation ultrasound images both in medicine and

industrial activity. In *pulse-echo* imaging the ultrasound image is generated directly from the back scattered information as described in [9]. Pulses are excited from an ultrasound transducer into a medium. Where the acoustical impedance (Z) change in the material, some part of the energy in the pulse will be reflected and the rest transmitted further into the medium. This process of energy transfer is described by the reflection (R_p) and transmission (T_p) coefficient given equation (2.12) and (2.13). The reflected part of the wave will have an attenuation factor due to loss and time delay at the receiver, known as *time of flight* (TOF). The TOF is the time used of by the wave to propagate back and forth to the transducer after it has been reflected at an interface:

$$d = \frac{ct}{2} \tag{2.20}$$

In this equation t is the TOF, d is the travel distance and c is the speed of sound. The combination of TOF and attenuation is the core information in *pulse-echo* ultrasonic imaging. With multiple interfaces of different impedance in the medium there will be a high number of reflections, these can be used to measure depth and speed of sound in multiple medium between interfaces and with signal processing generate an image. An example of ultrasound *pulse-echo* imaging is illustrated to the left in figure 2.3 and a received signal to the right. In the figure, the time of flight is illustrated in the received signal.

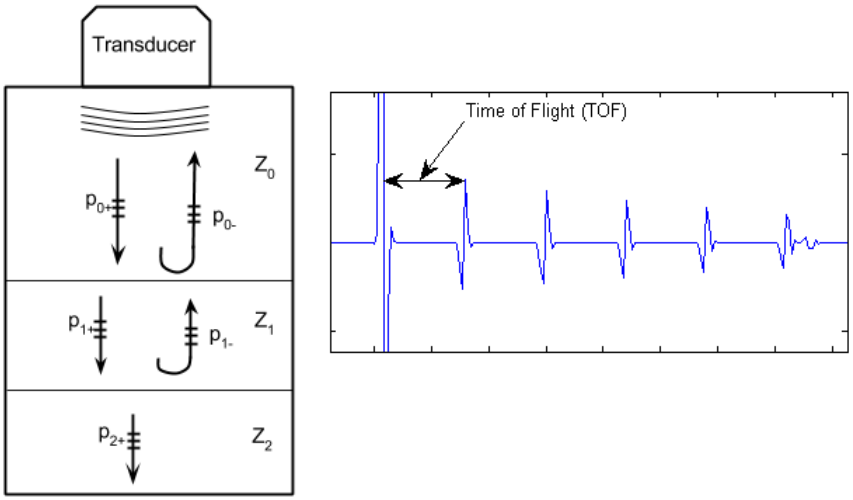

Figure 2.3: *Pulse-echo* setup (left) and a typical received signal (right)

In the *pitch-catch* method a source transducer and a receiver transducer are positioned in the same medium above a reflective interface with spacing between them. The source transducer will have an angular tilt, which let the waves have an incident angle else than normal incident. This is in order to have the possibility of exiting structural wave modes in the reflective interface. The receiver transducer will usually have the same angular tilt as the source. By positioning the receiver at different lengths apart for the source, it is possible to study direct reflections, scattering or wave modes in a solid layer. The technique is widely used in NDT, because of the possibility of exciting wave mode in structural materials and examining flaws [10].

2.2 SURF imaging

The effect of non-linearity has been shown to be significant for relevant intensities and frequencies used in ultrasonic biomedical tissue imaging [11]. This is particularly important when high pressure is applied and the tissue is no longer regarded as completely elastic. New imaging technique based on non-linear effects known as harmonic imaging has developed, with improved imaging quality [12]. One such method in biomedical imaging is known as *Second order ultrasound field* (SURF) [3], developed at the Department of Circulation and Medical Imaging (ISB) at NTNU. The method is a dual-frequency band technique, where pulses complexes composed of a low frequency (LF) and high frequency (HF) pulse are transmitted. Typical frequency ratio between the LF and HF pulse is 1:10, for instance a 0.1 MHz LF pulse and a 1 MHz HF pulse.

The background of SURF is that the non-linear effect described by equation (2.11) is decided both by the material parameters β and κ and the intensity p. The dual band SURF complex can be described in terms of a HF (y_{HF}) placed on a LF (y_{LF}) pulse. The idea is that the LF pulse manipulates the propagation properties of the medium, observed locally by the HF imaging pulse, due to the fact that these properties are dependent on the manipulation pressure. The LF pulse is often called the manipulation pulse. The use of a manipulation pulse leads to a high number of possibilities beyond that of harmonic self-distortion. For instance it is possible to place the imaging pulse at a positive or negative peak of the manipulation pulse and extract the harmonic image from the back-scattered information by signal processing.

A transmitted SURF complex ($y(t)$) can be described as a sum of the LF and HF pulse, in simple terms written as:

$$y(t) = y_{HF}(t) \pm y_{LF}(t) \tag{2.21}$$

By this equation it is observed that the HF imaging pulse can be extracted from the pulse complex by a bandpass filter. A model of a SURF complex is illustrated in figure 2.4. In this figure the two HF pulses are placed on a maximum and minimum peak of y_{LF}, denoted as $y_{HF}+$ and $y_{HF}-$. Since the speed of sound is dependent on the manipulation pressure $c(p)$, assuming constant material parameters, there will be a slight time difference between $y_{HF}+$ and $y_{HF}-$. It is possible to derive the theoretical time difference τ, by making some simple assumptions:

- Non-linear distortion of y_{HF} can be neglected
- The extent of y_{HF} is much smaller than one wavelength of the LF pulse, hence y_{HF} experience a constant manipulation pressure by y_{LF}

Making these general assumptions, the time difference caused by the non-linear effect as the wave propagates in a single medium from $z = 0$ to $z = L$ is theoretically [2]:

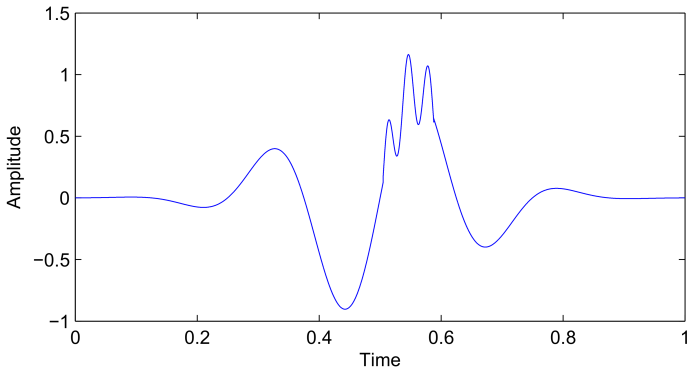

Figure 2.4: Surf complex: LF pulse with HF pulse positioned at a positive pressure peak.

$$\tau = \int_0^L (1/c_0 - 1/[c_0(1 + \beta\kappa p(z))])dz \tag{2.22}$$

In a simulation setting, the time delay τ between a non-linear and linear HF pulse, as illustrated in 2.5, can be estimated using cross correlation [13]:

$$Ry_1y_2(\tau) = E[y_1(t)r_2(t - \tau)] \tag{2.23}$$

where y_n represent the two signals which are delayed or ahead in time relative to each other, and E is the expectation operator.

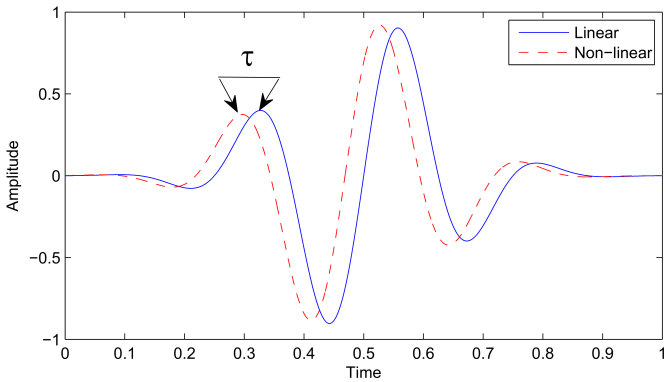

Figure 2.5: Time difference between linear and non-linear wave

The maximum peak output from (2.23) is where the correlation factor is the highest, and the estimated time delay is given by the argument of the maximum value of cross-correlation estimation:

$$\tau_{max} = \arg\max_{\tau}[Ry_1y_2(\tau)] \tag{2.24}$$

2.3 Finite Element Method

A physical system and its behavior can be described by a set of equations, governed by its geometry and its initial conditions and boundary conditions. These equations can be in the form of partial differential equations (PDE), characterized by containing unknown multivariable functions and their partial derivative. Performing a direct analytical analysis of complex physical systems can be very complicated, especially when the geometry is complicated and numerical methods are often favorable. *Finite Element Method* (FEM), also called *Finite Element Analysis* (FEA), is an effective numerical method for finding approximate solutions to boundary value problems and PDEs. FEM is used to analyze complex physical systems governed by PDEs, through discretization of the physical domain and the PDEs and ultimately approximate the solution of the PDEs with a given error tolerance. The general FEM solution process, can by some simplifications be described by the following five steps [14]:

1. Discretize the solution region into finite elements connected by nodes, this operations is often referred to as meshing.

2. Define interpolation functions to interpolate the field variable to be solved for over each finite element.

3. Find each elements properties by a set of matrix equations which relates nodal value to the unknown function, Galerkins Method is often used for this step.

4. Assemble the elements equations for all elements and solve the global matrix equation system by effective matrix calculations.

5. Compute desired physical quantities at selected elements in the model based on the global solution.

In this thesis, FEM is chosen as the preferred numerical method, because it can be a very effective and accurate method to simulate wave propagation and SURF has never been studied directly by using FEM. One of the topics will be to examine the possibility of simulating the SURF method by FEM. In order to be able to understand the processes involved in FEM, modeling accurate FEM studies and prevent numerical inaccuracies the main topics relevant to this thesis are described, which is discretization, Galerkin's method, time dependent analysis and modeling of non-reflective surfaces.

2.3.1 Discretization

The first step in solving a PDE numerically with the FEM method is the discretization the simulation domain Ω. This domain is divided into a number of M finite elements E_i called a mesh [15]. The conditions for placing the elements are that they do not overlap and that there are no empty spaces between them.

$$\Omega = \bigcup_{i=1}^{M} E_i \qquad \text{and} \qquad \forall i \neq j : Int(E_i) \cap Int(E_j) = 0 \tag{2.25}$$

This condition states that each finite element is interconnected at points called nodes, and N is the numbers of nodes in a mesh. Since the shape of the finite elements must satisfy the condition stated in equation (2.25), it is appropriate to use straight edges between each node. Thereby the most common shapes are polygons of either three or four corners of different shapes as illustrated in figure 2.6. There is always a node at each corner and possibly along the lines connecting the corners. The number of nodes is always equal to or larger than the number of corners. Another aspect is that meshing curves demand a high number of polygons to represent the domain. Generally, the quality of the final numerical solution depends on number of elements in the domain (i.e. the size) and their shape.

The core idea of FEM is that any shape can be approximated with an error by simple elements, this is illustrated in figure 2.6 where a three node polygon is used to approximate a circle.

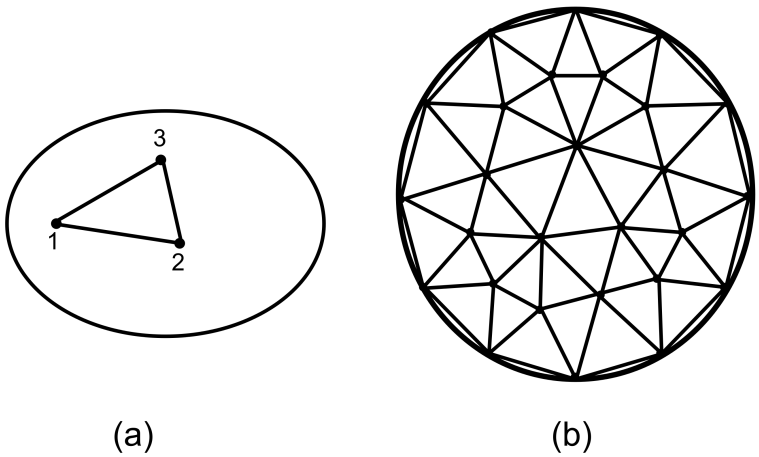

Figure 2.6: Three node polygon finite element defined in a domain (a) and a set of elements creating a mesh in the domain (b)

The solution of the PDE is calculated at each node of the mesh. If the finite elements in the domain are appropriately small, the discrete solution in each node can well be interpolated to non-nodal points by a simple function. This function is called an interpolation function or a shape function. To demonstrate the shape function we write a PDE in a general form:

$$\nu[u](x) + g(x) = 0 \tag{2.26}$$

Which is subject to the boundary conditions:

$$u(a) = u_a, \; u(b) = u_b \tag{2.27}$$

In this equation ν is an arbitrary second order differential operator. An approximate solution to this PDE can be the function $u(x)$, approximated by:

$$\tilde{u}(x) = \sum_{j=1}^{N} u_j N_j(x) = \left\{u^T\right\} \{N\} \tag{2.28}$$

where N is the number of nodes and, u_j is the value of the solution function at each node j and N_j is the corresponding shape function at that node. The summation is done over all nodes in the simulation domain. The shape function $N_j(x)$ can have an arbitrary shape, but need to have entity value at node j and 0 outside its respective element.

$$N_j(x_i) = \begin{cases} 1 \text{ for } i = j \\ 0 \text{ for } i \neq j \end{cases} \tag{2.29}$$

The simplest shape functions are linear functions or lower order polynomials, are also used in practical applications. Figure 2.7 illustrates the concept of shape functions. In the figure a continuous function u (black) is approximated by a linear polynomial $\tilde{u}$ (red) and the shape function N_i(green) inspired by [16].

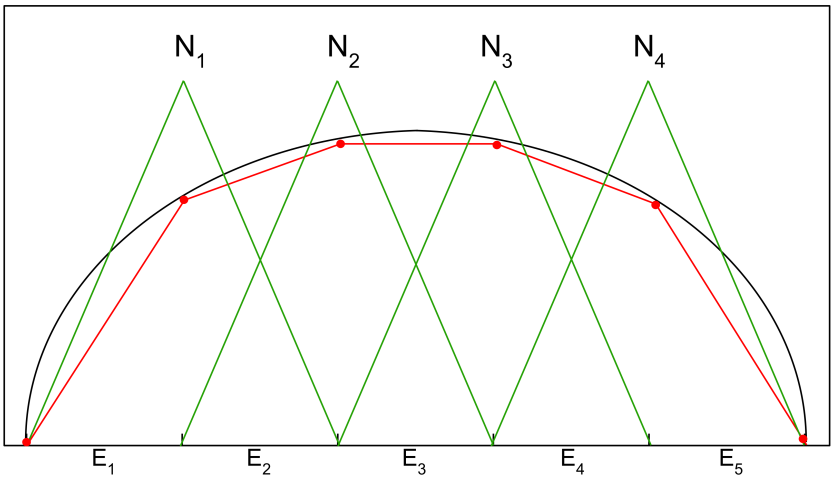

Figure 2.7: Function (black) approximated by linear polynomials (red) and their shape functions (green)

An important aspect of the interpolation is that it works well as long as the variable inside the element increases or decreases linearly. This is not the case for harmonic variations as with sinusoidal waves. This means that a high number of elements per wavelength is necessary to properly sample the variations of the wave. A rule of thumb states that there should be no less than six elements per wavelength, but the number can be higher for complicated geometries where much interaction between the fields occur [17].

2.3.2 Galerkins Method

By equation (2.28) it is desirable to construct a piecewise linear function $\tilde{u}(x)$ by the use of the shape functions $N_j(x)$ and the node values u_j. The object

is to find the optimal node values u_j so that the deviation between $\tilde{u}(x)$ and $u(x)$ is as small as possible. This can be done in many ways, but the most used method is the so called *Galerkin's weighted residual* method [15].

Substitution of the assumed solution in (2.28) into the differential equation gives the general residual:

$$R(x;u_j) = \sum_{j=1}^{N} [v[\tilde{u}] + g(x)] = \sum_{j=1}^{N} [v[u_j N_i(x))] + g(x)] \tag{2.30}$$

If the residual dissapear ($R = 0$) we obtain the exact solution and $\tilde{u}(x) = u(x)$. This solution does not exist in the general case. Therefore we try to fulfill the residual by an approximation, by the use of N weighted test functions $W_i(x)$:

$$\int_{\Omega} [W_i(x) R(x;u_j) d\Omega = 0, \qquad \text{for} \quad j = 1, 2, 3, \ldots N \tag{2.31}$$

In Galerkin's method the test function $W_i(x)$ is set equal to the shape function $N_i(x)$, resulting in:

$$\int_{\Omega} N_i(x) [\sum_{j=1}^{N} v[u_j N_j(x)] + g(x)] d\Omega = 0, \qquad \text{for} \quad j = 1, 2, 3, \ldots N \tag{2.32}$$

From this solution, it is possible to determine N unknown function values u_j, with a system of N equations by the use of integration by parts. This is the core computation in the FEM-method in a stationary analysis. Solving time dependent problems causes further complexity in the calculations, since there has to be added an additional integration and interpolation in time to the initial computation. This process is beyond the scope of this short introduction to FEM-calculations, but a further description can be found in [15] and [14].

2.3.3 Time Dependent Analysis

Solving time dependent problems causes further complexity in the calculations, since there has to be added an additional integration and interpolation in time to the initial computation. The details will be omitted, but some critical factors in a time dependent analysis are presented relevant for this thesis are presented. The convergence of the solution of a time depend problem is highly dependent on the geometric scales and the time scales involved in the system. These scales are both connected to physics involved and the numerical method of the solver. The scales have to be adjusted relative to these factors, to ensure a numerically accurate solution.

When solving the wave equation in the frequency domain, there is only one time scale set by the frequency as $T = 1/f$, but there are several length scales. The length scales are the wavelength λ, geometrical dimension L, the finite element size h and the thickness of the boundary layer δ. When solving the problem, it is important that the mesh is fine enough to both resolve geometries

and wavelength, without being too fine since there is a direct relation between element size and solution time. By using the condition of six elements per wavelength, the minimal elements size is:

$$h_{min} \leq \frac{\lambda}{N} \tag{2.33}$$

If the wave equation is solved in the time domain, the same considerations as for the frequency domain apply. The difference is in the new number of time scales which are introduced. That is the minimal wavelength resolution (i.e. highest frequency) and the time step Δt used by the numerical solver. A necessary condition to ensure numerical stability in the case of solving PDE by explicit time integration is the so called *Courant–Friedrichs–Lewy* number (CFL-number) [18]. This number relates the previously mentioned time step and element size as:

$$CFL = \frac{c\Delta t}{h_{min}} \tag{2.34}$$

Where c is the speed of sound and h_{min} is the minimal element size as defined in equation (2.33). COMSOL uses the second-order accurate generalized-α method to solve transient acoustics problems by default. Using this method, it is recommended that $CFL \leq 0.2$ to ensure convergence in the solution.

2.3.4 Modeling Non-reflective Surfaces

In a FEM simulation it is often desirable to simulate regions with no reflections or open boundaries (infinite extent). The problem with FEM is that the method is valid for definite area, not infinite areas meaning there will be reflections. However, there are methods to avoid this. In a transient study it is generally difficult to avoid spurious reflections, but it is possible in the case of normal incident plane waves. This is achieved by stating a plane wave radiation condition to a given boundary or by defining a medium where only one direction of propagation is possible. However the application of these methods is very limited, due to the previously mentioned restrictions.

For the case of a frequency domain study, the most applied technique is Perfectly matched layer (PML). The technique was initially developed for electromagnetic waves, but the technique works equally well for acoustic waves. The functionality of the PML is that it exponentially dampens incoming waves, leading to a strong absorption without reflections [19]. The difference between a PML and an absorbing material is that there is no reflections at the interface between the non-PML and the PML. The PML can have different forms with the possibility of absorbing both plane waves and spherical waves. In figure 2.8, a sinusoidal wave is hitting the boundary of an PML and is exponentially attenuated with no reflections.

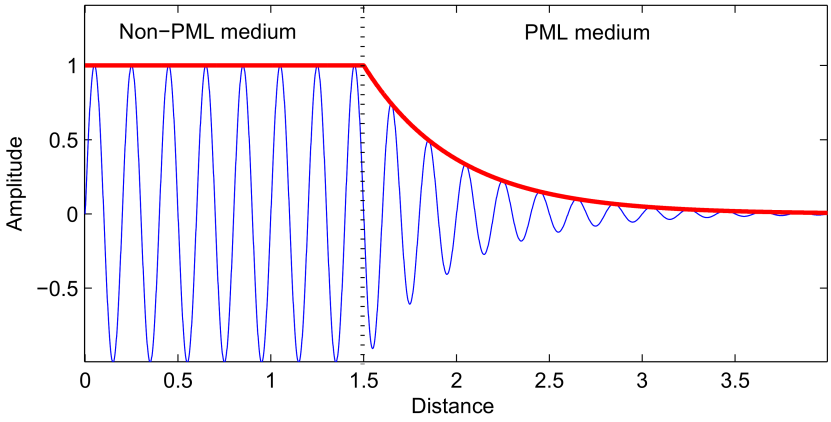

Figure 2.8: Wave attenuation within a PML

3 | Equipment

3.1 COMSOL

COMSOL Multiphysics is a general-purpose software intended to perform numerical analysis based on the FEM procedure of physic-based problems governed by PDEs. This software has been the core tool in this thesis to perform numerical simulations. COMSOL Multiphysics exists in several versions, in this thesis version 4.4 is applied. From now on COMSOL Multiphysics 4.4 is referred to only as COMSOL. The main reason why COMSOL is chosen as the software to perform the FEA, is that is does not require in-depth knowledge of mathematics or numerical analysis; it includes predefined interfaces for various physics and engineering applications. The interfaces include a great range of governing PDE's and boundary conditions for different physics. Nevertheless, COMSOL is highly flexible with the possibility of explicitly defining your own weak-form PDEs and physics. This allows both novice and experienced user to do simple and advanced simulations.

One of the key features in the program is the opportunity to couple different physical interfaces, making multiphysical simulations. The advantage of this is the possibility to include more unknown variable, inspect physical interaction and thereby do more accurate simulations. An example of a coupled interface is the *Acoustic-Solid Interaction* interface; this couples the acoustic wave equation with the governing PDEs in structural mechanics. With this interface it is easy to model ultrasound transmission through structures, as in this thesis. COMSOL is versatile in choosing possible studies; some of the possible studies are time-dependent, steady state frequency and Eigen frequency. To fully describe COMSOL and its details is considered to be unnecessary in this thesis. However, since it has such an important role, a more thorough description of the main features used in this thesis are provided.

3.1.1 Computer

COMSOL has certain computer demands which have to match the complexity of the model to be simulated. When a simulation is running, the program creates large matrices to handle the solution at each node as described in section 2.3. These matrices grow rapidly in size when handling high frequencies because of the condition to have at least 6 finite elements per wavelength. If a transient study is included the size grows even more, since a time variable is

added to each node. The resolution in the time domain is stated by the CLF-number in equation (2.34) which increases as a function of frequency. The result becomes that performing high frequency studies in the time domain are very computational demanding, especially regarding the memory usage. In this thesis a computer made disposable by Department of Electronics and Telecommunications and the Acoustic Group at NTNU is used. This is not a supercomputer, but capacities are above the average home computer, and enabling handling at least medium sized COMSOL models. The specifications of the computer used are given in table 3.1.

Table 3.1: System specification

Specification	
Computer name	aku-comsol1
Operating system	Windows Server 2012
System type	64-bit, x64-based processor
Memory	24 GB
Processor	Intel Xenon CPU E5520 2x2.27 GHz

3.1.2 Generate Study in COMSOL

The use of COMSOL to generate a model is similar to any other general-purpose finite element analysis (FEA) software as described in [15], and can be divided into three main steps:

1. *Pre-processing.* Define space dimensions, geometry and what kind of study to conduct. Based on this, one must define desired physics, boundary values and materials in the domain of study. In COMSOL this is easily done based on the built in physical interfaces, where you can choose standard conditions or replace them by your own. The next step is meshing the domain. COMSOL can do this automatically or let the user freely choose element, size and distribution to fit the domain. In this thesis a free-triangular algorithm is used and the size scaled to frequency and geometry. The last step in the pre-processing is to define study settings, like time domain, frequency domain and step size.

2. *Numerical analysis.* COMSOL automatically generates a solution based on the previously defined options. Matrices are generated, describing the behavior of each element in the domain. These matrices are combined to a large matrix equation representing the finite element structure, which is solved to provide the solution in each node. Substantial additional computations are done in the case of time-dependent studies, which is the case in this thesis.

3. *Post-processing.* The results from the numerical solution to dependent variable can be studied graphically directly in COMSOL or exported to another post-processing program, like Matlab.

The steps are illustrated in figure 3.1 where a domain has meshed with the free triangular algorithm, solved by a time dependent study and the solution is plotted as a propagating wave. Notice how the mesh is denser at complicated geometries, like around the hole in the middle of the domain.

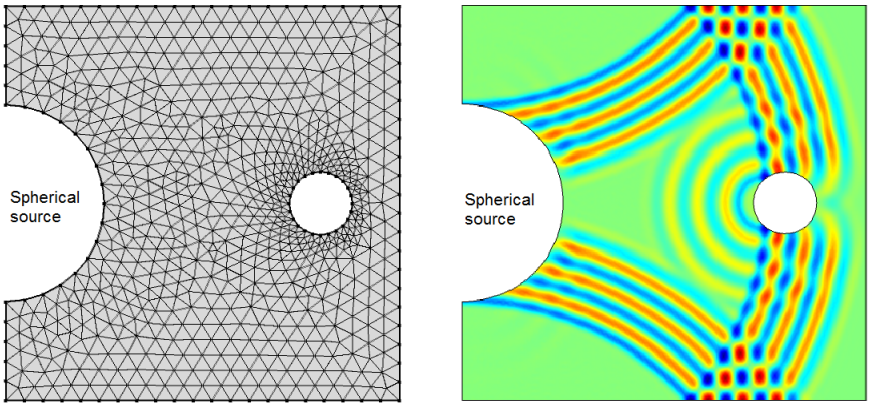

Figure 3.1: Time dependent solution with mesh and geometry (left) and snapshot of the simulated wave propagation (right)

Designing the geometry of a model in COMSOL can be done within the software itself, or by using a dedicated computer-aided design tool (CAD), for a simple geometry the built-in function works well. The most important aspect when designing a geometry is to consider possible symmetry, reduction of space dimensions (1D,2D...) and shrinking size. By use of these potential aspects, it is possible to save a large amount of computations, and thereby time. An additional aspect is to save key parameters as explicit definitions, making them easy to change. This enables the possibility to change the depth of layers in an acoustic transmission model.

The design of the geometry decides the domains and the boundaries separating each domain. In each domain a material must be applied. In COMSOL there is a large number of predefined material parameters which are linked to each physical interface. The value of the parameters can be freely chosen to fit any material. It is also possible to define custom materials.

3.1.3 Acoustic-Solid Interaction Interface

The most important part in the design of a COMSOL model it the choice of physical interfaces. The acoustic module in COMSOL includes a set of physics interfaces to model the propagation of sound in fluid and solids, described in [20]. The governing equation in the acoustic module is the classical wave equation which describes the acoustic field by one variable, the pressure:

$$\frac{1}{\rho_0 c^2}\frac{\partial^2 p}{\partial t^2} + \nabla \cdot (-\frac{1}{\rho_0}(\nabla p - \boldsymbol{q})) = \boldsymbol{Q} \tag{3.1}$$

where t is time, ρ_0 is density, and q and Q are the possible acoustic dipole and monopole terms. The four interfaces included are *Pressure Acoustics*, *Acoustic-solid Interaction*, *Aeroacoustics* and *Thermoacoustics*. Only the first two are applied in this thesis. The interfaces can analyze time domain and frequency domain phenomena. In the *Pressure Acoustics* interface the sound field is assumed to propagate in a fluid, where the dependent variable, which is solved for, is the pressure p. The *Acoustic-solid Interaction* interface is an extension to the *Pressure Acoustics* interfaces, where the fluid pressure causes a fluid load of a solid domain and the acceleration in the structure acts as normal acceleration in the fluid domain, this interface is coupled to the *Solid Mechanics* interface. The dependent variables in this interface is both the pressure p and the displacement field $\mathbf{u}$. With this dependent variable in addition and the coupling of the interfaces, the weak form PDE becomes more complicated and the solution time increases. When the *Acoustic-Solid Interaction* interface is selected to a set of domains, there are many possible features and boundary conditions to apply to the domains to govern the physics. In this chapter only the *Acoustic-Solid Interaction* interface is explained, since most of the discussion is valid for the *Pressure Acoustics* interface also.

3.1.3.1 Material Models

There are several different material models to replicate fluid or solid domains. It is not practical to mention all the available material models in the Ac*oustic-Solid Interaction* interface. The discussion is limited to the material models used in this thesis. In this thesis the linear elastic material model is applied both structural and fluid domains, unless else is stated. In a fluid domain the linear elastic material model have the governing parameters defining the physics, which are the speed of sound c and the density ρ. For a linear elastic solid interface an isotropic material is assumed and the material properties defining the elastic material properties are Young's modulus E and the Poisson's ratio v, which are parameters describing specific structural relationships. By the elastic material model it is possible to simulate structural waves in any solid defined by these parameters.

3.1.3.2 Initial Values

The initial value is a specified value of an unknown function at a specified time $t = t_0$. Given the initial values, the PDE becomes an initial value problem and is solved as an evolution from the initial values. This is also how the PDEs are solved in COMSOL, and defining initial values are mandatory. In the *Acoustic-Solid Interaction* interface the dependent variables are the pressure and the displacement field, the initial values are given by these parameters and their derivative as:

- Pressure p (Pa)
- Pressure, first time derivate $\frac{\partial p}{\partial t}$ (Pa/s)
- Displacement field u (m)

- Structural velocity field $\frac{\partial u}{\partial t}$ (m/s)

In this thesis all the given initial values are set to zero, resembling a system in relaxation.

3.1.3.3 Boundary Conditions

In a model it is necessary to define boundary conditions on every interface between domains [21]. These are important parameters in the solution of all PDEs and is also one of necessary elements in the solution by the FEM. Since the boundary conditions plays such an important role when defining a physical model, the most important boundary conditions implemented in the *Acoustic-Solid Interaction* interface and used in this thesis are described more in details. The documentation of the boundary conditions are retrieved from [20]. The condition *hard boundary* is a perfectly reflecting boundary or a wall, where the normal component of the acceleration is zero, thus all incoming waves are reflected with a 180 degrees phase shift.

$$-\mathbf{n}(-\frac{1}{\rho_0}(\nabla p - q_d) = 0 \tag{3.2}$$

The *Acoustic-Structure boundary* condition is only applicable to a boundary between a fluid and a solid and is the core of the *Acoustic-Solid Interaction* interface. The pressure load from the fluid act on the solid as defined by:

$$\mathbf{F}_p = -\mathbf{n}p \tag{3.3}$$

where the structural acceleration acts on the boundary between the solid and the fluid. The normal acceleration of the acoustic pressure p on the boundary is equal the second derivative of the displacement $\mathbf{u}$:

$$a_n = \mathbf{n} \cdot \frac{\partial^2 u}{\partial t^2} \tag{3.4}$$

A *plane wave radiation* condition adds a radiation of a plane wave at a boundary. This allows modeling a incident plane wave source as:

$$p_i = p_0 e^{-i(k \cdot r)} \tag{3.5}$$

where k is the incident wavenumber and r is the location of the wave. It is also possible to use this condition as a non-reflective surface to plane waves. The reflection from the layer is given as:

$$R_s = \left| \frac{cos(\theta) - 1}{cos(\theta) + 1} \right| \tag{3.6}$$

where θ is the incident angle, so at normal incident there is no reflections. The *Normal acceleration* condition adds an acceleration source condition to the boundary. This can be thought of as a piston moving back and forth, described as:

$$-\mathbf{n}(-\frac{1}{\rho_0}(\nabla p - q_d) = a_n \tag{3.7}$$

The particle acceleration a_n of a plain sound wave is coupled to the sound pressure p through the acoustic impedance Z by the relation:

$$a_n = \xi\omega^2 = v\omega = \frac{|p|\,\omega}{\rho c} = \frac{|p|\,\omega}{Z} \tag{3.8}$$

where ξ is the particle displacement, v is the particle velocity and ω is the angular frequency.

4 | Simulations

The goal is to implement the SURF technique described in section 2.2 by equation (2.11) into a FEM simulation environment in COMSOL. The key to achieve this is described by the equation for non-linear speed of sound (2.11). In this equation the speed of sound is dependent on the non-linear parameter β , the compressibility of the medium K and the pressure p. Assuming that the material parameters are constant in a homogenous and isotropic material, modifying the pressure is the remaining possibility to achieve non-linear wave propagation.

It is possible to modify the pressure in a stationary frequency study, but this has one major drawback. The nature of the frequency study is the complex representation of harmonic waves, the problem is to incorporate the non-linear speed of sound in such a study and difficulties with post-processing the results. This gives reason to assume that a time study of the SURF technique in COMSOL will be favorable, with the possibility to study time series and a more straight-forward implementation into the wave equation (3.1). A proposed method based on this discussion is given in the following chapter for time dependent studies. In order to verify the model, it is necessary to have several simulations, starting with simplest case of a small plane wave model in a single medium in 2D. Further, it is necessary with a model capable of handling different materials, both linear and non-linear, which is very relevant for *pulse-echo* ultrasound where structures of multiple materials are examined. The combination of these simple models is the foundation which can lead to more realistic and complex simulations, including mechanical structures and a realistic size of the simulation domain, with the aim of imitating the real measurement situation of steel pipes.

4.1 The Non-linear Speed of Sound Effect

To implement the proposed non-linear speed of sound effect, the governing weak form equation in COMSOL has to be modified. This has to be treated very carefully to avoid unwanted effects. The implementation method will be described in detail in the following section for the *Pressure Acoustics* interface and extended to the *Acoustic-Solid Interaction* interface, based on a suggested solution by the technical department in acoustics at COMSOL.

4.1.1 Pressure Acoustics Interface

The chosen study method for the non-linear effect is a time domain study, known in COMSOL as *Transient Study* in the *Pressure Acoustics* interface, where the dependent variable solved for is the pressure p, as described in section 3.1.3. In the SURF model two pulses y_{HF} and y_{LF} will be transmitted simultaneously with a frequency separation of 1:10. The LF pulse modifies the pressure in the material as a function of time and space $p(x,t)$, the space dimensions include y and z but this is omitted for simplicity. This change in pressure caused by y_{LF} is experienced locally by y_{HF}, propagating in the same medium. Since the change in pressure is dependent of time and space, the speed of sound in equation (2.11) will be dependent of time and space $c_0(x,t)$. In order to implement this in COMSOL, the idea is to use three *Pressure Acoustics* interfaces. Each interface will have an identifier in COMSOL, which makes it possible to link the interfaces with each other.

1. Interface for the LF pulse y_{LF}, with identifier *actd*.
2. Interface for the non-linear HF pulse y_{HF-NL} with modified speed of sound and identifier *actd*2.
3. Reference interface for the linear HF pulse y_{HF-L}, for comparison of y_{HF-NL} with identifier *actd*3.

Solving interface one *actd* using the linear speed of sound will result in a solution of the pressure $p = p_{LF}(x,t)$ within a given time sequence over the entire domain. When applying solution of the pressure p_{LF} when solving interface two *actd*2 for y_{HF-NL}, p_{LF} will act as a modulation pulse as described in the SURF method. Depending on the location of y_{HF} on y_{LF}, the HF pulse will experience a slight change in the speed of sound because of the modulation pressure caused by y_{LF}, defined by equation (2.11). A pressure above the ambient pressure p_0 leads to a higher speed of sound for y_{HF-NL} than the reference speed of sound c_0, and opposite for a pressure below the ambient pressure. There is a fundamental problem in this method caused by the governing weak form expression of the *Pressure Acoustics* interface,the weak form expression of equation (3.1) is defined in COMSOL as:

```
(-actd2.gradp(x,y,z)*actd2.gradtestp(x,y,z)...
-d(d(actd2.p_t,t),t)*test(p2)/actd2.c_c^2)/actd2.rho_c
```

In this expression, *grad* is the gradient operator and *test* is the test function for the numerical integration, as described in the FEM theory. The identifiers *actd*2.*p_t*, *actd*2.*c_c* and *actd*2.*rho_c* are references to the pressure, speed of sound and density in physical interface number two. These parameters are from the defined arbitrary materials parameters in a model. The expression is solved for the pressure defined by p_2. When the expression is solved for the pressure, it is assumed that the speed of sound is only spatially dependent, $c_0 = c_0(x)$. This makes it possible for the solver in COMSOL to extract the speed of sound from the time derivative, given by the d operator in the

expression. However, this not the case for the situation described above, as the pressure is dependent on both time and space $p(x,t)$ and thereby also the speed of sound $c_0 = c_0(x,t)$ and it is not possible to extract from the derivative in interface two, the way COMSOL usually handles the speed of sound. To overcome this, it is necessary to define a new variable in the physical interface:

```
rho_user = actd2.p_t/(actd.c*...
(1+mat3.def.beta*actd.p_t/(actd.c^2*actd.rho)))^2
```

This variable makes COMSOL able to solve the wave equation with the time dependent speed of sound including the non-linear term on line two. Including this variable in the original weak form expression and rearranging the terms give a new weak form expression for COMSOL to solve:

```
(-actd2.gradp(x,y,z)*actd2.gradtestp(x,y,z)...
-d(d(rho_user,t),t)*test(p2))/actd2.rho_c
```

The expression states that the speed of sound is included in the derivative by the term *rho_user*. Also the LF pressure defined by y_{LF} as *actd.p_t* is included to give the pressure dependent speed of sound. To solve this expression in COMSOL, it is necessary to modify the solver, since there is a direct dependency between the physics interfaces *actd* and *actd*2. The resulting linear system is solved using the solver known as multifrontal massively parallel sparse direct solver (MUMPS). This solver is a version of Gaussian elimination for sparse systems of matrices often arising is the finite element method. To ensure stability and full connection between the interfaces, it is necessary to solve the two physics interfaces simultaneously and use a fully coupled solution combined with the direct MUMPS solver. The fully coupled solvers option of 'Jacobian update' must be set to 'on every iteration'. In general FEM, the Jacobian matrix is used for transformation of coordinate systems and updating this on every iteration improves convergence in time dependent studies in COMSOL.

4.1.2 Acoustic-Solid Interaction Interface

In section 3.1.3, it is described that the *Acoustic-Solid Interaction* interface is an extension of the *Pressure Acoustics* interface with an additional dependent variable, the displacement **u**. The derivation of the non-linear speed of sound in the *Pressure Acoustics* interface is therefore the foundation of the implementation of non-linear speed of sound in the *Acoustic-solid Interaction* interface and will only be described briefly.

Since there is an additional dependent variable in the acoustic structure interface, there is also an additional weak form expression. COMSOL has implemented the *Acoustic-Solid Interaction* interface by combining two interfaces, the *Pressure Acoustics* interface and the linear elastic material model from the mechanics-interface. Each of these interfaces have their own weak form expression to couple the individual physics into a multiphysical model. The weak

form expression in the linear elastic material model can remain unchanged in this study, since it is assumed to be linear with no SURF effects. The weak form expression in the *Pressure Acoustics* interface needs to be changed in the identical manner as in the previous section. The difference is the new identifier for the *Acoustic-solid Interaction* interface *astd* and an increased number of terms. By defining a new *rho_user* and substitute the original expression for the pressure *astd.p_t* within the time derivative, the speed of sound is included in the derivative as in the previous section. The original and modified weak form expression is found in the appendix A. Also, this implementation has to be solved simultaneously for *astd* (y_{LF}) and *astd2* ($y_{HF-nlin}$) by using the fully coupled solver.

4.2 Source Signal

In a time dependent FEM study involving high frequency components, it is necessary to take into consideration the risk of numerical artifacts. The theory in section 2.3.3 describes how the time steps of the solver Δt has to be linked to minimum element size h_{min} by equation (2.34) and the CFL number, to prevent artifacts. Even though this condition may be fulfilled, some situations have to be given special attention regarding the frequency components of incident waves.

The source signal in this thesis has to be chosen wisely because of the high frequency component in HF pulse in the SURF pulse complex. A pressure pulse with a very steep inclination in the time domain will lead to its derivative increasing towards infinity and generates high frequency components, observed as side lobes in the frequency domain. One possible way to refine the source signal is to append a window function, also known as a weighting function. To illustrate this, consider three pulses, first a simple sinusoid:

$$y_{HF}(t) = |p| \sin(2\pi f_0 t) \text{ for } 0 < t < 2t_0 \tag{4.1}$$

where $|p|$ is the pressure amplitude, f_0 is the center frequency and t_0 is the pulse length. The sinusoid in equation (4.1) can be regarded as the fundamental frequency of the signals. A sine weighted sinusoid is achieved by smoothing the fundamental period of the signal by a half period sinusoid (half frequency) as:

$$y_{HF}(t) = |p| \sin(\pi f_0 t) \sin(2\pi f_0 t) \text{ for } 0 < t < 2t_0 \tag{4.2}$$

Another possible signal is to use a Gaussian weighting function. The shape of the Gaussian curve is given by its mean and variance, and result in the typical bell shape. To simplify the expression it possible to use an approximation of the Gaussian with variance of one:

$$y_{HF}(t) = |p| e^{-(\pi f_0 (t - \frac{1}{2f_0}))^2} \sin(2\pi f_0 t) \text{ for } 0 < t < 2t_0 \tag{4.3}$$

The pulse shapes are plotted in figure 4.1 a center frequency 1 MHz. The fundamental sinusoid is presented in figure 4.1 derived from equation (4.1). By applying a weighting function to the fundamental signal as in equation (4.2) and (4.3), the start and end of the pulse are smoothed off as shown in the figure. This is favorable from a numerical analysis perspective, because steep inclinations are computational difficult to evaluate.

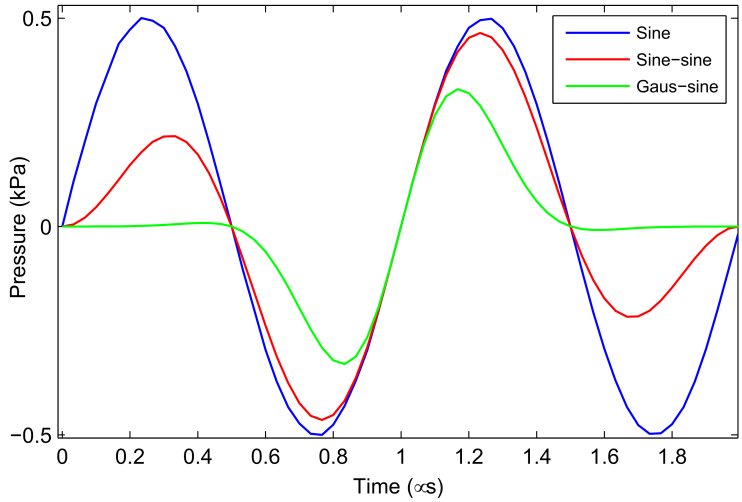

Figure 4.1: Source signals in the time domain

The frequency spectrum of the signals are plotted in 4.2. Because of the fundamental signal given in equation (4.1), the center frequency is at 1 MHz. The simple sinusoid has side lobes repeating themselves above the fundamental frequency. This is not ideal because it will lead to numerical artifact if the mesh in the simulation is tuned to 1 MHz. The sine weighted sinusoid have tendencies to side lobes at 2 MHz and 2,8 MHz, while the Gaussian weighted sinusoid has no side lobes and falls off gradually.

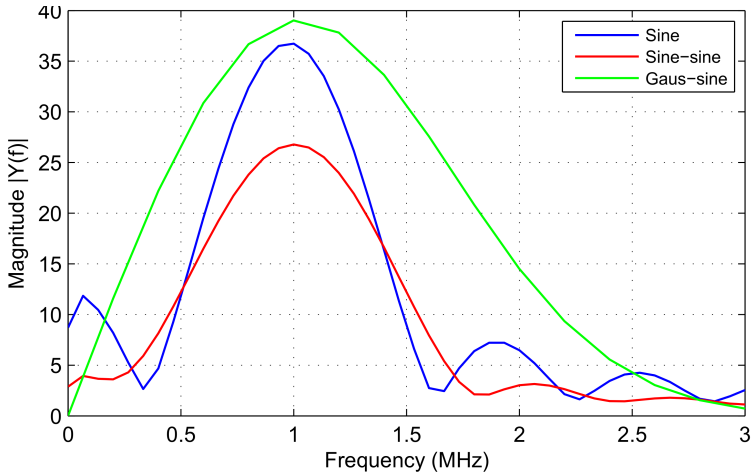

Figure 4.2: Source signals in the frequency domain

It is possible with a wide variety of windowing functions to suppress side lobes and achieve different signal shapes, but to go further in this analysis is beyond

this thesis, and simulations made in this thesis uses the Gaussian weighted sinusoid for the high frequency component.

4.3 Non-linear Plane Wave Model

In order to verify the modification made to the *Pressure Acoustics* interface described in section 4.1.1 it is necessary with a simple model which is easy to evaluate. The simplest case may be an acoustic plane wave channel with hard walls, without loss and terminated with $z = \rho_0 c$ impedance with minimal reflections. The model setup and geometry is shown in figure 4.3.

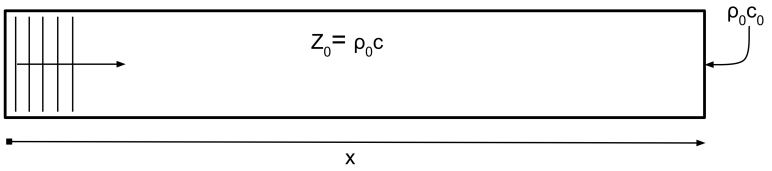

Figure 4.3: Plane wave channel

The most important thing when choosing the length of the model in the x-direction is that it is long enough for considerable non-linear delay to occur. Choosing a length of $x = 7$ cm will result in considerable delay, if the modulation pressure in the LF pulse is high enough. The y-scale is set to two wavelengths long, it is thin to have a smaller computational domain. Since the model is a basic ultrasound transmission model, the material model is a fluid with water as the material and parameters given in table 4.1.

Table 4.1: Material specification

Parameters	**Water**
Speed of sound $[m/s]$	1495
Density $[kg/m^3]$	1000
Compressibility $[Pa^{-1}]$	$447e^{(-12)}$
Non-linear par.	5

Most of the considerations regarding numerical accuracy of the source pulse is presented in section 4.2. In this model two identical pulse shapes are used for y_{LF} and y_{HF} with a frequency separation of 1:10 as stated in the SURF technique. The source signal parameters are presented in table 4.2. The most important aspect in this model, is that there is high enough pressure amplitude of y_{LF} to get sufficient modulation, and thereby non-linear time differences as stated by equation (2.11). The amplitude of y_{HF} should be small enough to consider no non-linear distortion. The HF pulse should be placed on a positive or negative peak of y_{LF} for maximum modulation.

Table 4.2: Source signal specification

Parameters	y_{LF}	y_{HF}
Centre freq. $[MHz]$	0.1	1
Pressure $[kPa]$	330	0.1
Signal shape	Eq. 4.3	Eq. 4.3

4.4 Non-linear Plane Wave Multiple Materials

In a multilayer transmission model, it is desirable to be able to include an arbitrary number of materials. By including several non-linear materials it is possible to express the materials as variables in the COMSOL environment. Each variable can be set to be valid for any chosen number of user-defined domains. By this technique, models with different non-linear materials are fairly straight forward to set up. However, it is necessary to verify the use of this technique before using this model to any other simulations. A simple, but yet important model is a three layer structure of different medium. This is an extension to the model in section 4.3 by including two more domains. The model implemented is illustrated in figure 4.4 where the leftmost layer is water, the middle layer is steel and rightmost layer is an artificial non-linear material. The length of the layers are stated as L_n. For all simulations $L_0 = 6\lambda_{LF}$, $L_1 = 0.6\lambda_{LF}$ and $L_2 = 2\lambda_{LF}$. The boundaries surrounding the model are hard reflecting surfaces, except for the plane wave radiation condition and the ρc termination. This model is a simple scheme to evaluate the results from the multiple non-linear materials case. It is also possible to extend the model with some simple modification to examine some important physical aspects when applying ultrasound SURF, this will be described later on.

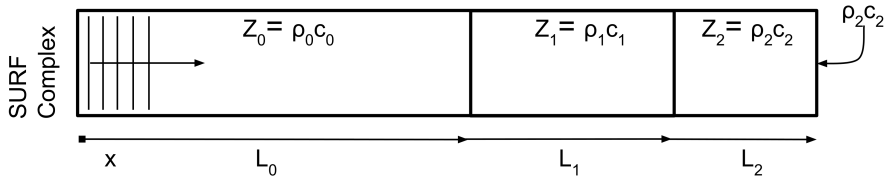

Figure 4.4: Two layer transmission

The material parameters for the model is given in table 4.3. In this model the steel is modeled as a fluid with zero compressibility and thereby no non-linear effects. Assuming that the steel layer is a fluid, is implicitly stating that there are no structural waves modes in the layer. This is a significant simplification to neglect other wave modes in some situations, but this is accurate enough for this simple transmission model. The artificial material has the same density and speed of sound as water, but with a non-linear parameter of $\beta = 20$. Thereby y_{HF} will have much higher change in the speed of sound. The choice of an artificial material is justified by the fact that this is only a proof of concept. The parameters defining the source signal are summed up in table 4.4. The LF

signal in this model is a sinusoid; this is to be able to build up the pressure over several periods by extending the signal length. The signal parameters are valid for all simulations made on this model. Using the given model as a foundation and doing some small changes it is possible to examine several phenomena. The model is extended to simulations on half-wave resonance and standing waves (SW) as described in the next two subsections by time-dependent analysis.

Table 4.3: Material specification for multiple materials model

Parameters	**Water**	**Steel**	**Artificial**
Speed of sound $[m/s]$	1495	5970	1495
Density $[kg/m^3]$	1000	7790	100
Compressibility $[Pa^{-1}]$	$447e^{(-12)}$	-	$447e^{(-12)}$
Non-linear par.	5	-	20

Table 4.4: Source signal specification

Parameters	y_{LF}	y_{HF}
Centre freq. $[MHz]$	0.1	1
Pressure $[kPa]$	500	0.1
Signal shape	Eq. 4.1	Eq. 4.3

4.4.1 Half Wavelength Resonance

In order to examine the materials behind the steel plate using SURF in *pulse-echo* setting, it is crucial to have as much transmission through the steel plate into the bottom NLL as possible. However, the material parameters give a large impedance difference at the interface between water and steel indicating high reflection at the water-steel interface. Inserting the material parameters of water and steel into equation (2.12) gives a reflection coefficient of $|R| \approx 0.94$. The reflection coefficient states that only 6% of the acoustic energy is transmitted to the steel layer. With almost no transmission there will be a low modulation pressure in the non-linear layer.

One possible way to ensure transmission is to apply impedance matching between the layers. Equation (2.15) states that it is possible to have almost full transmission if the frequency of the signal or the length of the steel layer is matched to a half wavelength. In this simulation the most practical way to do this is to modify the length of the middle layer L_1 to match the frequency of y_{LF} by $L_1 = n\lambda_{Lf}/2$. Another aspect is that y_{LF} need to be several periods long, so that the pressure in the middle layer has time to build up at the resonance frequency as described in 2.1.3. The length of y_{LF} is chosen to be 8 periods long, the other signal parameters are summed up in table 4.4. In order to examine the half wavelength resonance the middle layer L_1 is chosen

according to the center frequency of y_{LF}, also the case of quarter wavelength and a arbitrary length are implemented for comparison. In these simulations, the bottom layer is terminated with ρc. The lengths defining the model are then:

- $L_0 = 6\lambda_{LF}$
- $L_1 = \lambda_{LF}/2,\ \lambda_{LF}/4,\ \text{and},\ 0.35\lambda_{LF}$
- $L_2 = 2\lambda_{LF}$

4.4.2 Standing Waves

In a real situation it may not be realistic to satisfy the half wavelength resonance criterion of the middle layer. However, when a long y_{LF} is transmitted and the bottom layer is terminated with a highly reflective surface $|R| \approx 1$ it is possible to build up standing waves in the bottom non-linear layer L_2. This is the same physical principal as the half-wave resonance and is the result of interference between waves propagating in opposite direction creating a stationary wave pattern. This can possibly cause y_{HF} to propagate under the influence of the LF pulse in both directions under resonance pressure. If positive interference is achieved between the forward and backward propagating wave, a higher manipulation pressure and thereby larger time delays from the bottom NLL is achieved. There are also other factors which determine the modulation of y_{HF}, such the phase of y_{HF} in reference to y_{LF}. However, deciding the optimal length L_2 and the phase relationship is not a trivial task. The simplest case, studied in [4], of a single layer ended with a reflective surface suggests the length of the layer to be an integer number of half wavelengths and a phase of zero in reference to the y_{LF} peaks. However the situation examined in figure 4.4 is a multilayer structure with different reflection and transmission constraints, so the studies give no great insight. A multilayer structure is examined in [4] and the optimal length L is indicated to be $L = \lambda_{LF}(0.4 + n/2)$. The resonance is not at half a wavelength, but is half wavelength spaced apart. At this length SW is generated in the bottom layer, however the text states that the phase relationship is difficult to determine.

By examining how the LF pressure in the bottom layer is behaving for different L_2, it may be possible to decide when the pressure is at the greatest in the SW case. To simplify the analysis, the same model as in figure 4.4, but the end is terminated with a perfectly reflecting surface defined by equation (3.2). Firstly only y_{LF} is simulated by varying the length of L_2 to find maximum manipulation pressure in the bottom layer. The lengths of the model in the simulations are:

- $L_0 = 6\lambda_{LF}$
- $L_1 = \lambda_{LF}/2$
- $L_2 = 2\lambda_{LF},\ 1.9\lambda_{LF},\ 1.75\lambda_{LF}$ and $1.8\lambda_{LF}$

Deciding the optimal length of the bottom layer in terms of the wavelength of y_{LF} where the LF pressure in the bottom is the greatest, is important to be able to examine the NLL behind the steel plate. In order to examine the bottom layer, medium 0 and 1 in figure 4.4 is set to be linear, so there will be no time delay generated. The only time delay generated between the linear and non-linear y_{HF}, will therefore originate from the bottom layer and this delay may be observed at the receiver. The idea is that with proper SURF signal processing at the receiver you can observe the delay and then estimate the degree of non-linearity in the material behind the steel interface.

4.5 Non-linear Pulse-echo Simulation

Ultrasound imaging through structural steelpipes is a much more complex situation than the previously described models. In the previous model steel is considered to be a fluid and therefore only pressure waves are examined. In most situations this is a coarse simplification, since there will always be elastic body waves in the any structural element. Also, the previous model has small extent the in y-direction leading to a quasi 1D model. The true situation is a full scale 3D model with all dimensions to scale, including a realistic source model of an ultrasound transducer. However, this is considered to be beyond the scope of this thesis and steel pipe is simplified to a 2D steel interface. Another aspect is that from a numerical computational perspective, it is unrealistic to run simulations on a 3D domain using the FEM with the given computational power employed for this thesis. However, many 3D physical phenomena can be studied very well with a 2D model, partly because of axis-symmetrical geometries which also to some extent is valid for this thesis. Based on this discussion, a 3D model of a steel pipe is simplified to a 2D model of a steel interface, with realistic dimension related to a possible NDT-scheme with ultrasound transmission through steel pipes.

4.5.1 Normal Incident Pulse-echo Simulation

The model is a three layer structure of water as the first layer, steel as the second layer and water as the third layer. An ultrasound transducer is submerged into the first layer placed directly above steel layer illustrated in figure 4.5 with dimensions and applied boundary condition stated. The water layers are modeled as fluids as in the previous models. The middle layer is modeled as a structural steel layer to resemble a steel pipe, implemented by the Acoustic-solid interaction interface in COMSOL. This interface couples the acoustic pressure to the mechanical displacement at the boundary between the fluid and the structure as described in section 3.1.3. The mechanical part of the Acoustic-solid interface makes it possible to study new wave modalities in the fluid layers caused by deformations in the structural layer. The transducer is modeled as a 2D acceleration source resembling a moving piston, an adequate approximation to a true transducer in this simulation. The source signal generated by the transducer is the same as stated in table 4.4. The study in this

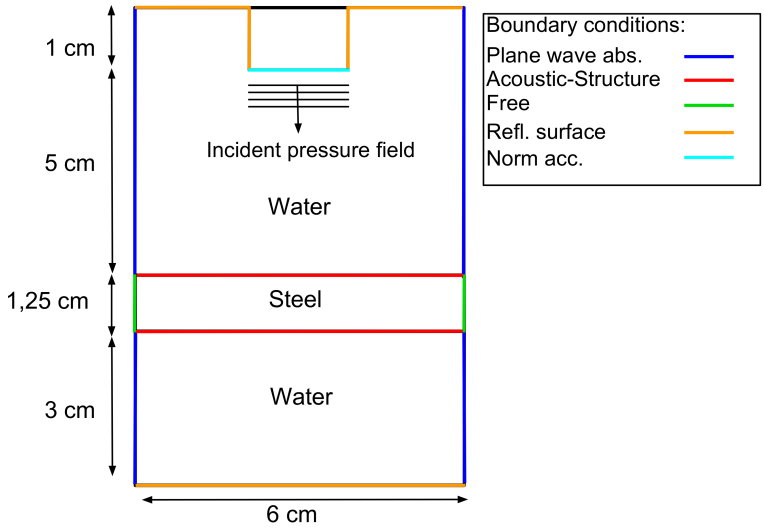

Figure 4.5: *Pulse-echo* model for time domain studies with applied boundary conditions

model is of plan waves, so the dimensions of the model are scaled to be within the range of the near-field of the transducer, where plane waves are assumed. The near-field limit can be approximated by the center frequency f of the signal and the diameter D of the transducer [9] as $N = D^2/4\lambda$. With the diameter of transducer being 3,5 cm, the near field limit is $N \approx 0.2m$. The boundary conditions applied to the model are reflective surfaces as defined by equation (3.2) on the top boundary, bottom boundary and the transducer structure. The horizontal walls on the side are set to absorbing surfaces. The steel plate boundaries are set to 'free', allowing the plate to move in all directions and the transition between the fluid and solid is set to the acoustic-structure boundary condition defined by equation (3.3) and (3.4).

Table 4.5: Material specification Acoustic-solid model

Parameters	**Water**	**Steel**
Speed of sound $[m/s]$	1495	5970
Density $[kg/m^3]$	1000	7790
Compressibility $[Pa^{-1}]$	$447e^{(-12)}$	-
Non-linear par	5	-
Poisson's ratio	-	0.33
Young's modulus $[GPa]$	-	200

In order to study this model it is considered appropriate to perform time and frequency domains study. The time domain study is most suitable to study the time series of reflected and transmitted pressure, and is also the most practical way to analyze the results in time-delay estimation, pulse distortion and interference in a SURF scheme. The frequency domain study is a highly suitable way to study steady state frequency dependent phenomena, like transmission and reflection coefficients which is important in a SURF study. The

frequency domain study is also the least computationally heavy, if the modeled is designed wisely. The frequency domain models are based on the model '*Acoustic Transmission Loss through Periodic Elastic Structures*' in the built in COMSOL model library [22]. The model computed in the frequency domain in COMSOL is illustrated in figure 4.6.

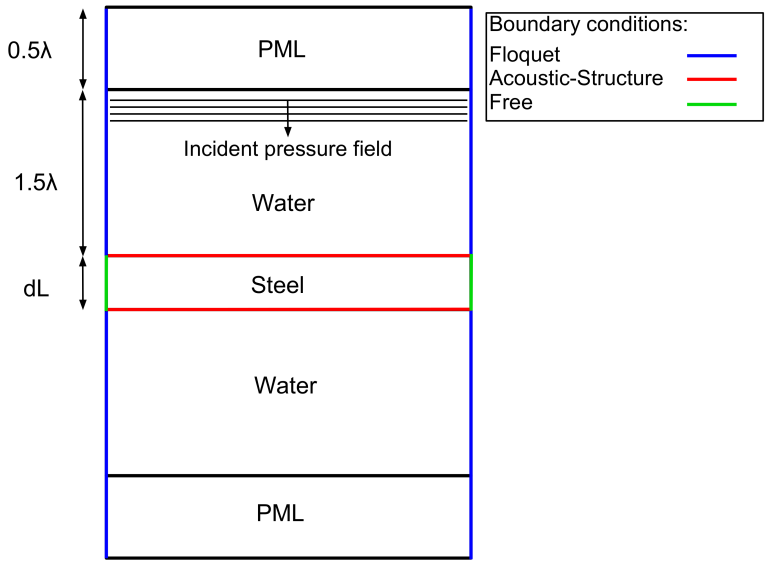

Figure 4.6: Normal incident *pulse-echo* frequency domain study with boundary conditions

In the top right corner of the figure, the employed boundary conditions are stated. The Floquet condition states that the solution can be sought in the form of two functions, one following the periodicity of the structure and the other the periodicity of the incident pulse realized by a vector $\mathbf{k}$ [21]. By the use of this periodicity, it is possible to extend the solution periodically for improved post-processing capabilities. The model is terminated with PML at the top and bottom to prevent reflections described in section 2.3.4. By relating the scale of the figure to the wavelength, it is possible to have a distributed mesh with a mesh resolution fitted to the frequency i.e. 10 elements per wavelength, and thereby ensures convergence in the solution.

4.5.2 Arbitrary Incident Angle with Pitch-catch

Pitch-catch is a general term describing a measuring setup where the acoustic energy is transmitted from one transducer and received by another on the same or opposite surface. This adds an extra degree of freedom compared to the normal incident cases, since it is possible to tilt the source and receiver transducer at any angle. As a result of the tilted incident angle, the ultrasonic waves will have much more complicated traveling paths due to the reflection angles. In this simulation the model setup is presented in figure 4.7. Here a source transducer modeled as an acceleration source and a receiver a computational cut-line, submerged into a water layer above a structural steel layer

and another water layer, with the same material models and parameters as in section 4.5.1 given in table 4.5. The transducer to the right in figure 4.7 can be tilted by the angle θ, which is also possible for the receiver.

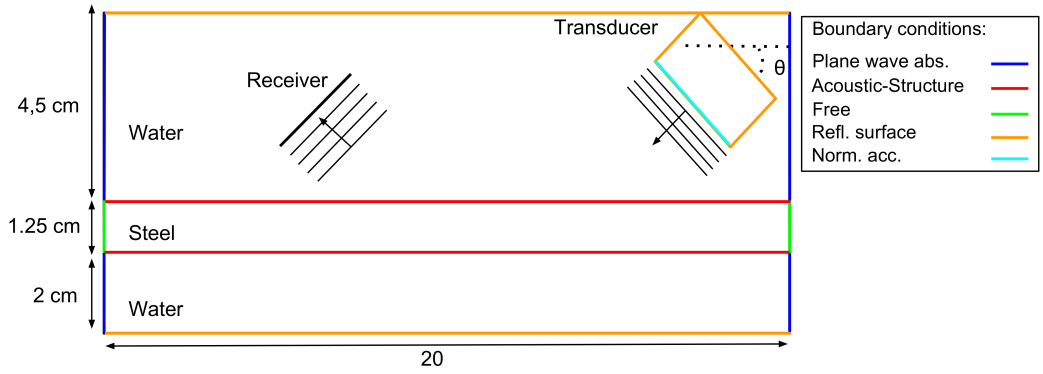

Figure 4.7: *Pitch-catch* model for time domain studies with dimensions and applied boundary conditions

To examine the non-linear layer behind the steel plate it is necessary to have as much transmission as possible, but this is difficult to achieve since the impedance different between water and steel is very high. In the case of normal incident waves, equation (2.14) states that a steel layer of half wavelength gives the lowest input impedance and highest transmission, but this is only true for normal incident waves. Generally the transmission and reflection coefficient at an interface is highly dependent on the incident angle in addition to the material parameters. The input impedance and transmission coefficient will therefore be a function of incident angle, material parameters, layer thickness and frequency. There are analytical expressions for these coefficients which are, at least valid for compressional and shear waves in the steel layer shown in [8]. However, in this analysis there may be other wave modes exited in the structural layer including plate bending, which can excite compressional waves into the fluid layers and further complicate the analysis of transmission. One important aspect in a SURF scheme is then to find the angles for y_{LF} where the transmission is the greatest. In order to study the transmission and reflection as a function of the incident angle θ at the steel-water interface, a frequency domain study is the most practical and least computational difficult. The model illustrated in figure 4.8 is an extension of 4.6 where the incident angle is changed, while the frequency is kept constant.

As mentioned earlier, the optimal position of the receiver transducer can be difficult to decide, because of multiple reflection possibilities directly from the structure, reverberation within the structure, plate bending and reflection from bottom layer. This is not possible to study with a steady-state frequency study, but has to be studied in the time domain. The simulation made in the time domain will be time series of transmitted and reflected pressure in *pitch-catch* mode with variable receiver distance and source angle. The simulations in the

frequency domain will be transmitted and reflected pressure as a function of incident angle.

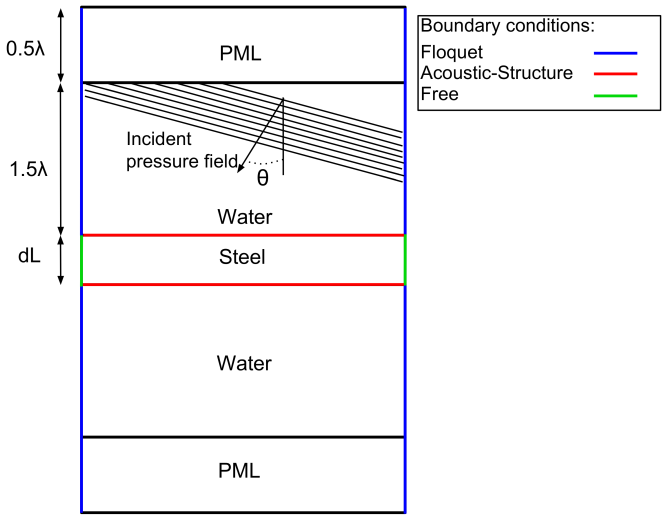

Figure 4.8: Arbitrary incident angle for*pitch-catch* model for frequency domain study with applied boundary conditions

5 | Results and Discussion

5.1 Non-linear Plane Wave Model

The non-linear plane wave model is a simple study of non-linear speed of sound and a validation of the modifications made to the physics interface in COMSOL. The modifications of the interface are specified in section 4.1.1, and the model is described in section 4.3. As y_{HF} propagates in the plane wave channel, it is expected that the pressure variation caused locally by y_{LF} relative to the ambient pressure will slightly modify the speed of sound of y_{HF} by the relation of pressure and non-linear speed of sound described by equation (2.11). Figure 5.1 shows the pulse at end of the channel, and a lower travel time is indicating higher propagation speed. The figure is a snapshot of y_{HF} and y_{LF} at $t = 35\ \mu s$, included is y_{HF} which is propagating with linear speed of sound for comparison. From this figure it is hard to see any real time difference between the linear and non-linear wave, but this is expected because of the short travel distance and low non-linear parameters β.

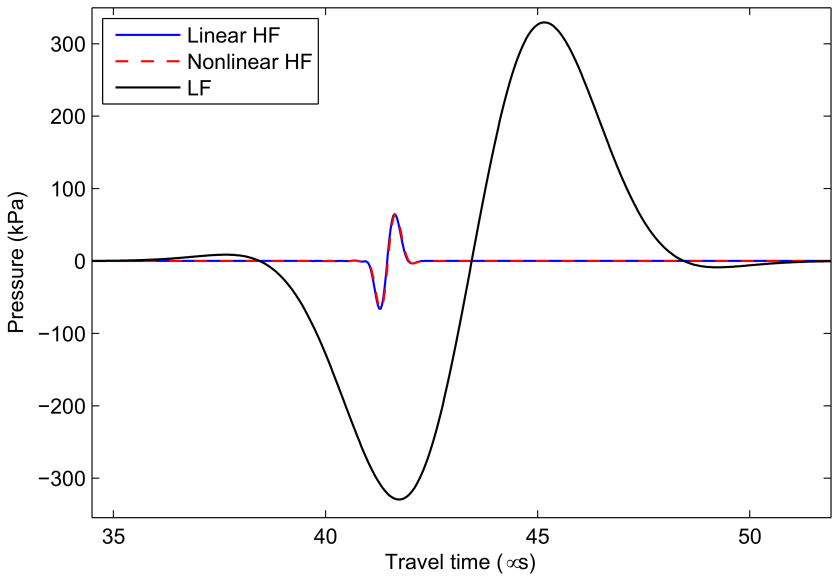

Figure 5.1: Simulated SURF complex with the LF pulse, the linear HF pulse and the non-linear LF pulse

By inspecting the linear and non-linear y_{HF} isolated as in figure 5.2, the time difference between the waves are clear. When the non-linear y_{HF} is locally

experiencing the pressure variation caused by the negative peak of y_{LF}, the speed of sound of the non-linear y_{HF} is decreased. This is observable in the figure, as the nonlinear wave is behind in time of the linear wave at the end of the plane wave channel.

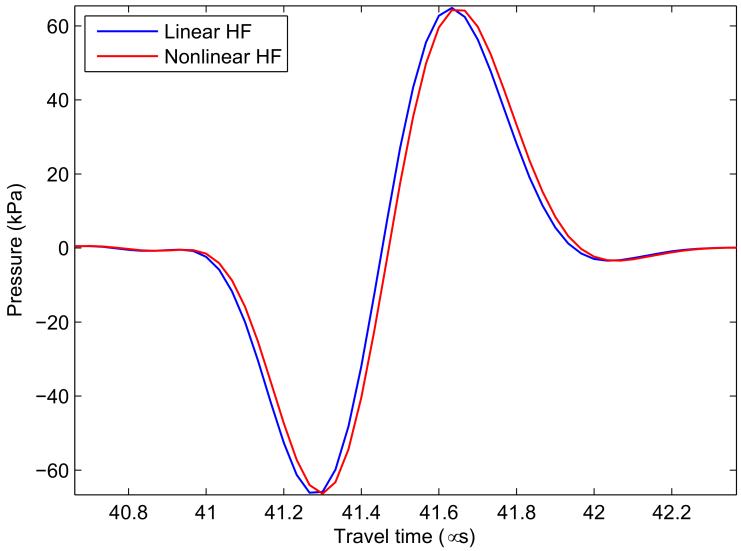

Figure 5.2: Plane wave time difference between linear and non-linear HF pulse

The time delay will increase over time, and lead to growing difference between the linear and non-linear wave. In this simple plane wave model with fixed maximum pressure amplitude, the effect is easy to verify, since the time difference between the linear and non-linear y_{HF} is explicitly given by equation (2.22).

The plane wave channel length is 7 cm, and the time difference is calculated from the simulations using the cross-correlation technique described in figure (2.23) is compared to the theoretical calculated values in figure 5.3, with a modulation pressure of 330 kPa. There is a very good match between the simulated and theoretical values, showing the linear relationship between travel distance and accumulated time difference, deviations are very small and in the range of nanosecond. In COMSOL there is an essential difference by the time-step taken by the solver and the time-step given by solver output. Even though the time step within the solver itself may give an accurate solution with proper sampling, the output may not, and leads to small differences between the simulated and the theoretically calculated value.

5.2 Non-linear Plane Wave Multiple Materials

The COMSOL implementation of a multiple material SURF scheme is described in section 4.4. The case is very much similar to the case described in the one-material implementation, but with one main difference, as the speed

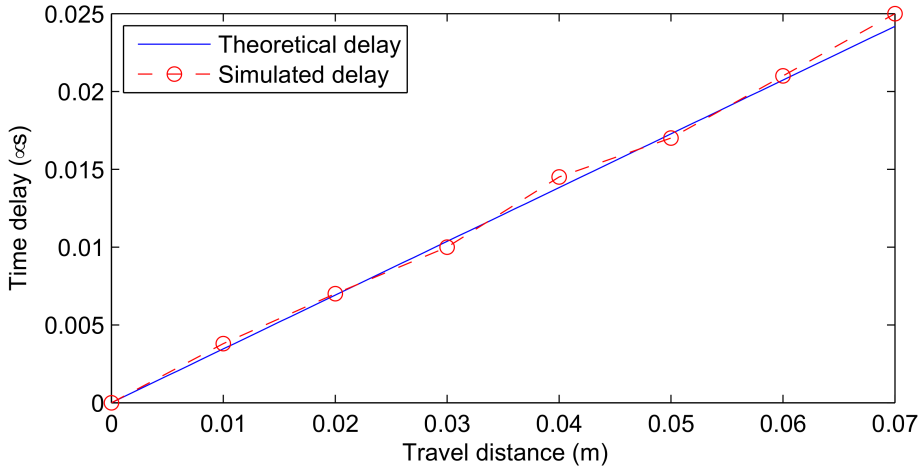

Figure 5.3: Non-linear delay over distance in the plane wave channel

of sound varies of each material of a multimaterial model. When some of the materials have non-linear properties and others not, the modulation of the non-linear y_{HF} is varying. By introducing a linear fluid steel middle layer with $\beta = 0$ and an artificial fluid bottom non-linear layer with $\beta = 20$ the resulting simulated time delay is calculated over travel distance. The simulated pressure distribution over the geometry of the model at the times 0.04 ms, 0.06 ms and 0.08 ms is plotted in figure 5.4.

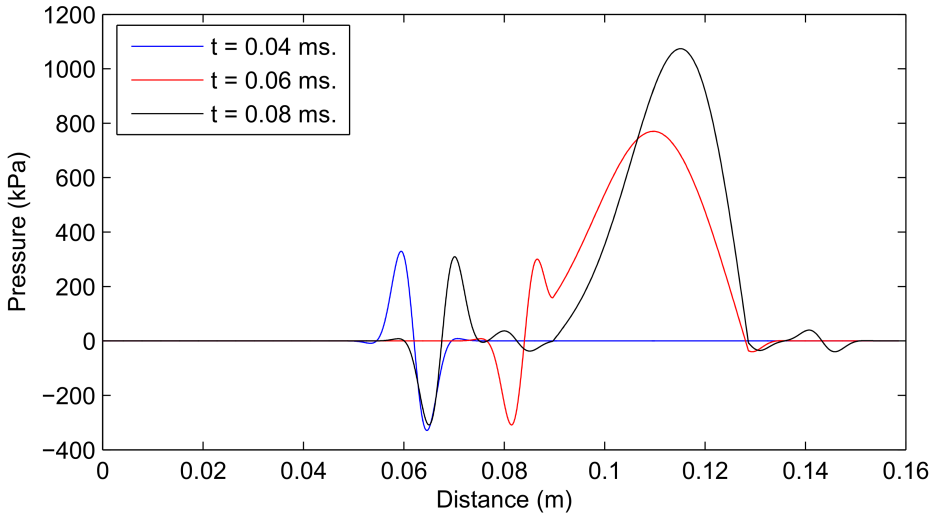

Figure 5.4: Pressure distribution of y_{LF} over the model geometry defined by figure 4.4 in simulations at time t_n

In the figure, the initial pressure of y_{LF} is 330 kPa at $t = 0.04$ ms. At $t = 0.06$ ms, y_{LF} has been transmitted through the first water-steel interface, and the pressure is building up within the steel layer to approximately 800 kPa. The pressure of 40 kPa at $t = 0.08$ ms is the transmitted pressure to the bottom layer, which implies a transmission coefficient of $T \approx 0.12$ at the interface resulting in very little modulation, even though the non-linear parameter is 20.

To calculate the theoretical time difference, it is not enough to know each of the non-linear parameters, but also necessary to know the modulation pressure in each medium, since the modulation pressure is not equal to the excitation pressure after transmission through the steel layer, as shown in figure 5.4. The modulation pressure can be extracted directly from the COMSOL simulations or by calculating the reflection and transmission coefficient analytically by equation (2.14), but this can be difficult with resonances. In this simulation the pressure is extracted from the COMSOL simulation, and is used to calculate the theoretical delay. In figure 5.5, the simulated and theoretically calculated time differences are plotted as functions of travel distance. The theoretical and simulated values are matching very well, and as observed in the figure there is no manipulation in the steel layer as desired. The result shows that the multiple material model is validated as correct, because the simulated delays are as predicted by SURF. The small deviation between the simulated and theoretical values may be the result of the same factors as discussed in the previous section.

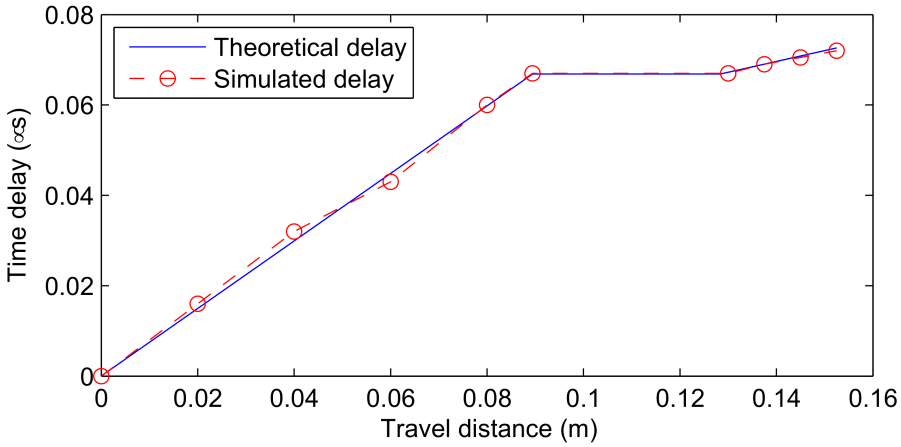

Figure 5.5: Nonlinear delay in materials with different degree of non-linearity $\beta_n = 3.5$, 0 and 20.

One important result of this simulation is that it demonstrates the fact that the transmitted pressure to the bottom non-linear layer (NLL) is very low. This is expected due to the large impedance difference between water and steel, which results in a high value of the reflection coefficient. This is crucial to take into consideration if the bottom NLL is to be examined, especially in a SURF study where it is favorable to have as much time difference as possible between the linear and non-linear wave.

5.2.1 Half Wavelength Resonance

As described in the model description in section 4.4 and demonstrated in figure 5.4, it is difficult to observe any considerable transmission through the steel layer. Based on theory presented in section 2.1.3, it should be possible to have high transmission by matching the frequency or the thickness of the steel layer to the wavelength. This is necessary in order to have modulation pressure for

imaging pulse y_{HF} in the bottom NLL. Using a pulse length for y_{LF} of several wavelengths, the pressure will build up within the steel layer because of the positive interference, and result in high modulation pressure in the bottom layer. In the simulation, the thickness of middle layer set to $L_1 = \lambda/2$ and $L_1 = \lambda/4$, and pressure at the inlet and end is calculated. The time series at the inlet are plotted in figure 5.6 for both $L_1 = \lambda/2$ and $L_1 = \lambda/4$. The plot shows a significant difference between the two layer thicknesses. For a quarter-wavelength thickness, the amplitude reflection coefficient is $R \approx 0.94$, which is almost total reflection for the whole 8-cycle pulse length. With a half wavelength layer thickness, the initial reflection coefficient is also $R \approx 0.94$, but as the pressure builds up in the middle layer, the transmission is increasing over the total pulse length.

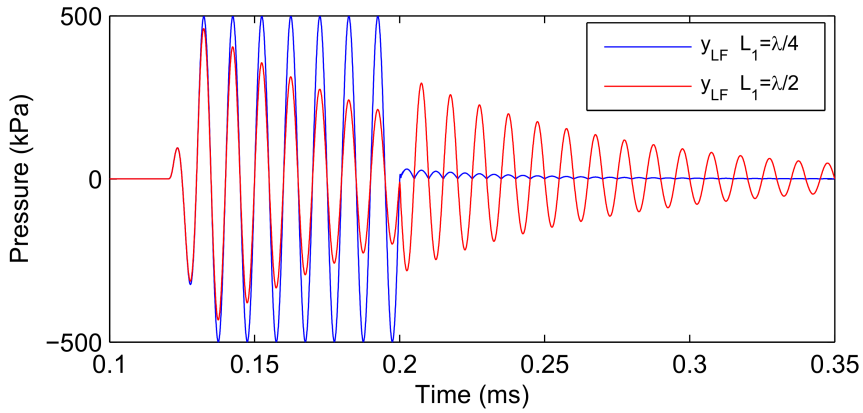

Figure 5.6: Pressure at inlet of y_{LF} for middle layer length of $L_1 = \lambda/2$ and $\lambda/4$

At the transition between the directly reflected wave and the reverberations, there is a phase shift of 180 degrees of y_{LF}. Imagine a *pulse-echo* scheme where the imaging pulse y_{HF} is being transmitted on a positive pressure peak of y_{LF} propagating in the positive x-direction. When y_{LF} is reflected and phase shifted, y_{HF} will propagate in the negative x-direction on a negative pressure peak. The result is the positive and negative pressure will counteract each other and the total modulation of y_HF is zero at the receiver. This is not a problem in through transmission, but can be very unfavorable in a *pulse-echo* SURF evaluation. The complementing time series at the end shows the pressure in the bottom NLL, which is plotted in figure 5.7 for both $L_1 = \lambda/2$ and $L_1 = \lambda/4$. It seems clear that the transmission increases over the pulse length, as indicated in figure 5.6.

By comparing the plot from the inlet and the end, it seems clear that the half-wave resonance provides an increasing pressure in the bottom layer over the pulse length. When the whole 8 cycle pulse has been transmitted the pressure in the bottom layer is 300 kPa, which is a transmission coefficient $T \approx 0.6$. The pressure distribution over the geometry at $t = 0.1348$ ms and $t = 0.0833$ ms is plotted in figure 5.8. The figure shows that pressure is building up within the steel shown as the peak at $x = 0.11$ m, which is in the middle of the steel

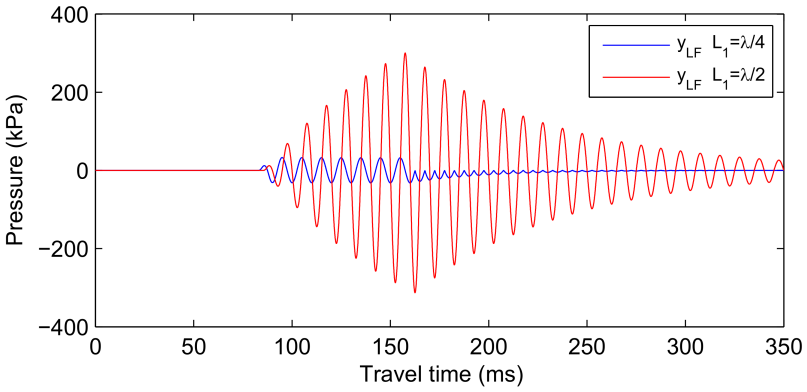

Figure 5.7: Pressure at right most endpoint of the plane wave multiple material model

layer. In the right part of the figure, the transmitted pressure have built up over the pulse period of y_{LF} to a much higher value than the initial pressure caused at $t = 0.12348$ ms.

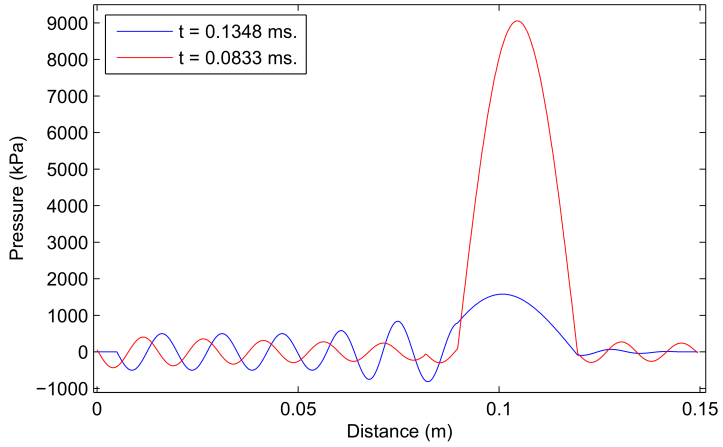

Figure 5.8: Half-wave resonance pressure distribution

5.2.2 Standing Waves

Section 4.4.2 describes simulations on several bottom NLL thicknesses. The simulations have proved achieving a stable SW pattern in the bottom for the lengths $L_2 = 2\lambda_{LF}$, $1.75\lambda_{LF}$ and $1.8\lambda_{LF}$ to be difficult. The pressure distribution with a bottom layer thickness of $L_2 = 1.9\lambda_{LF}$ is plotted in figure 5.9. The plot shows a SW pattern with nodal point spaced $\lambda_{LF}/2$ apart. It is also noticeable that the maximum pressure amplitude is 550 kPa, which is higher than the transmitted pressure amplitude of 500 kPa, even though this is after the transmission through the steel layer. This clearly demonstrates that it is possible to build up substantial LF pressure in the bottom layer, even after transmission through steel.

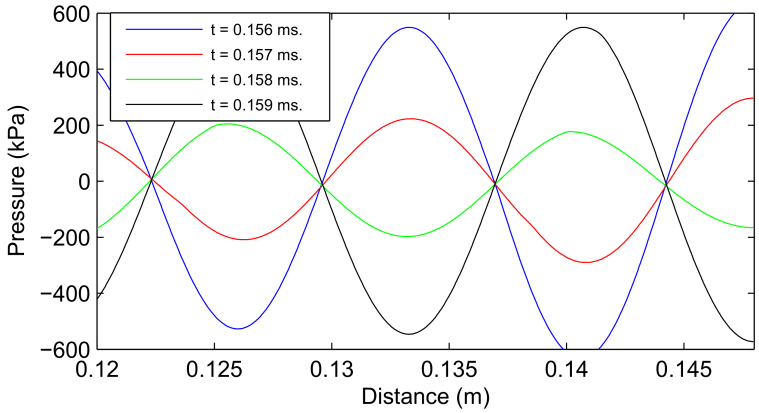

Figure 5.9: SW pressure distribution of y_{LF} at time in the bottom NLL

A problem with the case of SW in the bottom layer is how the SW pattern interacts with the imaging pulse. It is possible that y_{HF} will end up in a negative phase of the SW pattern even though y_{HF} was transmitted on a positive peak at the source. This effect will counteract the positive modulation in the top layer, and there may be little or no total modulation from the bottom layer. Figure 5.10 shows the pressure distribution over the bottom layer with length $L_2 = 1.9\lambda$ at time $t = 0.1465, 0.152$ and 0.157 ms. The same SW pattern as in figure 5.9 is observable. The more interesting observation is that the y_{HF} is propagating under the influence of positive pressure in both directions, resulting in maximum modulation.

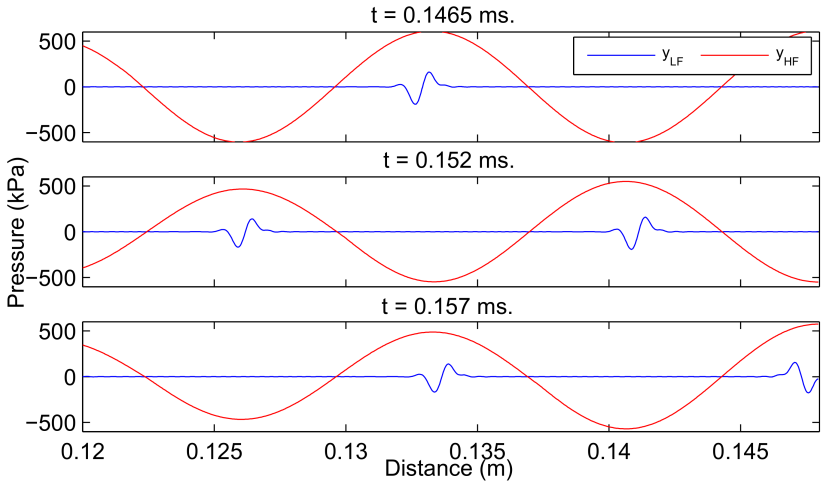

Figure 5.10: SW where y_{HF} is propagating under the influence of y_{LF}

In the SURF processing scheme, all mediums are linear except for the bottom layer. At the receiver there will be a high number of reflections, both of interest and no interest. In this study, the reflections from the bottom NLL are of interest to evaluate if there is time difference at the receiver. In figure 5.11, the pressure distribution over the geometry is plotted for three time values specified in the figure. In the top plot, y_{HF} has propagated from source on the left hand side with y_{LF} for time $t = 0.08$ ms The pressure within the steel

layer has started to build up, and there is little transmission of y_{LF} at this time. In the middle plot at time $t = 0.14$ ms, three waves originating from y_{HF} are observable: the direct reflection, the wave within the middle layer and the transmitted wave in the bottom layer. The LF pressure in the bottom layer has now built up to 450 kPa In the bottom plot, the reverberations from the steel layer are observable at the negative pressure peaks, spaced one wavelength apart. At distance $x = 0.061$ m and 0.078 m the reflections from the bottom layer are observable, ahead in time of the reverberations from the steel layer. By these plots it is hard to spot the time difference generated by the non-linearity in the bottom layer.

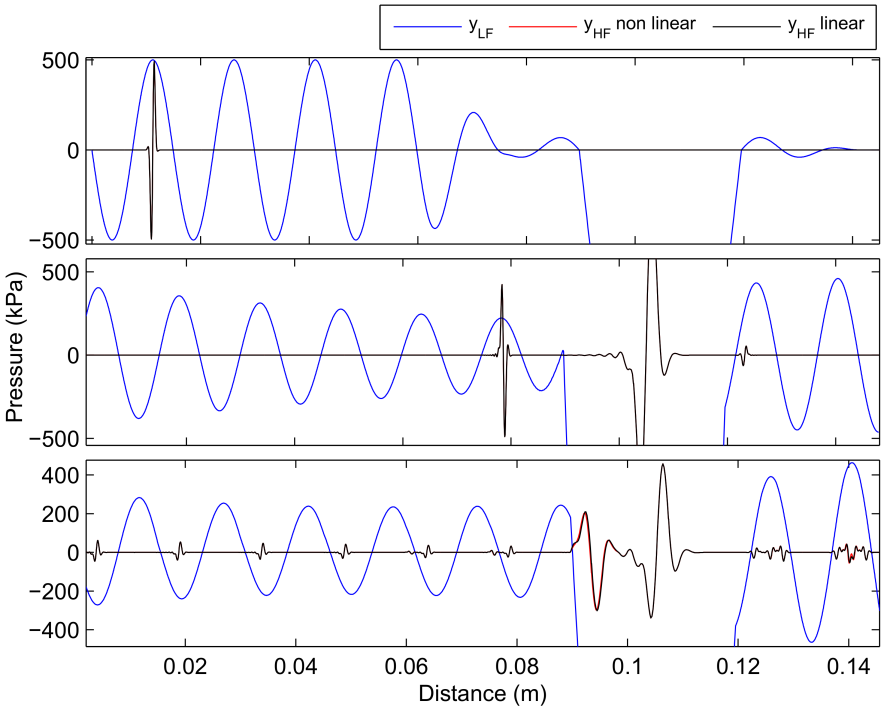

Figure 5.11: Pressure distribution at time $t_1 = 0.08$ ms (top),$t_2 = 0.14$ ms (middle) and $t_3 = 0.2$ ms (bottom)

Figure 5.12 is a magnification of figure 5.11 at $t = 0.2$ ms. This shows y_{HF} reflected from the steel layer and y_{HF} reflected from the bottom layer. Comparing the linear and non-linear plot, there is a time difference in y_{HF} from the bottom layer, originating from the non-linear speed of sound in the bottom layer. This result shows that it is possible to detect delays from the non-linear layer behind steel. In a real measuring situation, advanced signal processing will be used to extract the reflections from the non-linear layer from reverberations. By this processing, it is possible to estimate the degree of non-linearity in the non-linear material and reduce noise.

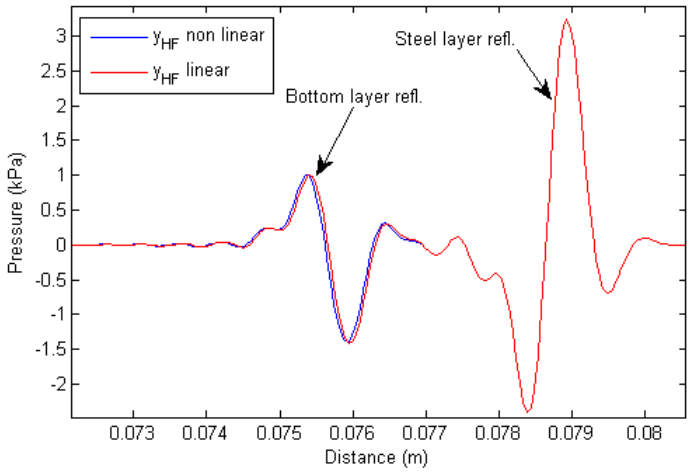

Figure 5.12: Delay from bottom NLL

5.3 Non-linear pulse-echo Simulation

Theses simulations are an attempt to take into consideration more factors by using the Acoustic-solid interaction interface, with the aim to have more realistic simulations of ultrasound transmission through steel than in the previously described models, as described in section 4.1.2. The studies of these models are done in both the time domain and frequency domain, due to the complexity of the computations and for easier analysis.

5.3.1 Normal Incident - Frequency Domain

The normal incident model is described in figure 4.6. In the simulation of transmission of reflection coefficient in the frequency domain, it is possible to examine the influence of structural waves in the model, and compare the coefficients against theoretical values. There are explicit analytical expressions for the transmission and reflection coefficient for a three layer structure ended by two semi infinite mediums, as given by equation (2.17) and (2.19) in section 2.1.3. In figure, 5.13 the simulated and theoretical calculated transmission and reflection coefficient are plotted as functions of frequency with a layer thickness of half a wavelength of $dL = 2.985$ cm (frequency 0.1 MHz), with a bottom layer ended with an absorptive boundary. The deviations between the simulated and analytical solution are very small and is not to be considered of significance. The result also reflect the half wave resonance as demonstrated in section 4.4.1. The good match between the theoretical and simulated is a not expected, since equation (2.17) and (2.19) are only valid for plane pressure waves in all medium, while the simulation uses a structural model for the steel layer. However, the simulations are plane waves at normal incident and the simulations indicate that other structural wave modalities does not have a great contribution. By changing thickness to $L_2 = 1.25$ cm the thickness of the structure is more than halved. The theoretical reflection and transmission coefficient, still match the simulated values, and demonstrate the half wavelength

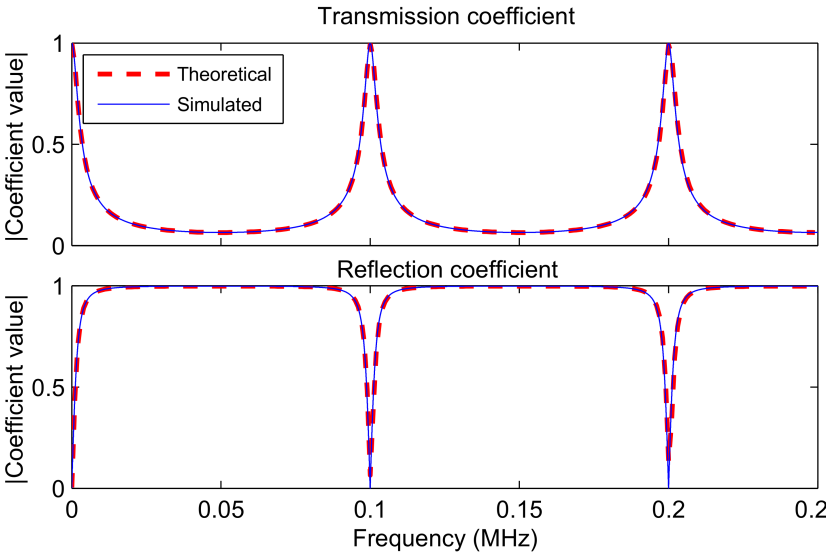

Figure 5.13: Transmission and reflection coefficient steel $dL = 2.985$ cm.

resonance at 0.24 MHz as described in figure 5.14. The structural behavior of the steel layer does not seem to have much effect for the transmission of sound waves at normal incident, and for thick layers in reference to wavelength, based on the simulations with non-reflective surfaces on the top and bottom of the model.

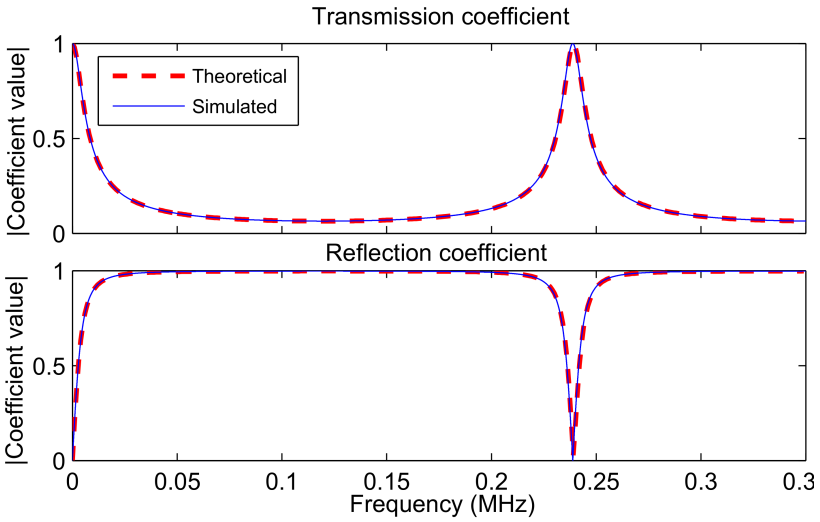

Figure 5.14: Transmission and reflection coefficient steel $dL = 1.25$ cm.

5.3.2 Arbitrary Incident Angle - Frequency Domain

The described model setup for *pitch-catch* in section 4.5.2 is a much more complicated setup to analyze, due to the complexity of arbitrary incident angle and the excitation of various waved modes in the structural steel layer. In addition, the model dimensions and thereby the computation time of the

FEM solution have increased. Because of the increased complexity the frequency domain study is chosen for some of the simulation. Additionally the reflection and transmission coefficient may be influenced by several resonances in the structural steel. In a SURF scheme to investigate the layer behind the steel plate, it is essential to identify the angles of greatest transmission.

In figure 5.15, the reflected and transmitted pressure of y_{LF} through a steel layer of $dL = 1.25$ cm (half-inch) are plotted. There are two incident angle of high transmission, one dominating angle where the transmission is the greatest at $\theta = 37$ degrees, and a smaller transmission peak at $\theta = 15$ degrees. An additional observation is that the transmission is very sensitive to the incident angle, i.e. the area of high transmission is very thin.

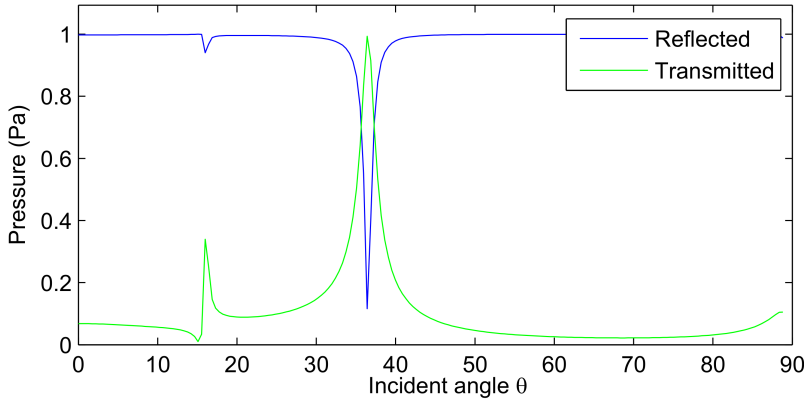

Figure 5.15: Reflected and transmitted pressure for y_{LF} for oblique incident angle

Figure 5.16 shows the total pressure distribution over the domain, and the deformation amplitude is plotted for the resonance incident angles $\theta = 15$ degrees and 37 degrees. At $\theta = 15$ degrees it is not possible to identify any resonance wave modes, in the plate and there is low transmission to the bottom layer. When $\theta = 37$ degrees there is almost full transmission to the bottom layer, there are deformations in the steel layer both in the direction of the wave propagation and perpendicular to the plane of the plate. These are familiar types of deformation to anti symmetric Lamb waves of the lowest order in plates and layer with free boundaries, as is the case in this simulation. Lamb waves are flexural waves, which can be exited several in different modes, where the symmetric and the anti-symmetric modes are the most common [23]. These wave modes are especially known to be exited in steel plates. They have been introduced to non-destructive ultrasonic testing [24] as they are very sensitive to abnormalities such as cracks. The criterions for the excitation of these are given by the frequency and the plate thickness for different modes. There are analytical expressions for these relations, but they are complicated especially for oblique incident waves and are not evaluated in this thesis.

With the angle of the greatest transmission for y_{LF} identified, it is also useful to know how the incident angle affects the transmission and reflection of

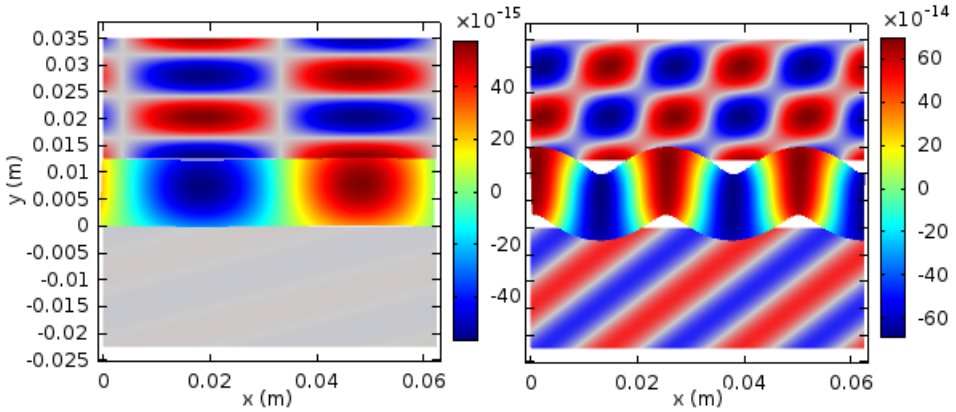

Figure 5.16: Pressure distribution and scaled plate deformation amplitude in the y-direction

y_{HF}. The idea is that y_{HF} and y_{LF} have to be transmitted at the same angle, but there is a possibility that there is an incident angle where both the pulses have great transmission. Using the same model as for y_{LF}, the transmitted and reflected pressure have been simulated for y_{HF}. The results are presented in figure 5.17. In this figure seven resonance angles with different degrees of transmission can be seen. This indicates that wavelengths small compared to the plate thickness excites several more wave modes in the plate. The result may be as seen in the figure with a great number of resonance peaks.

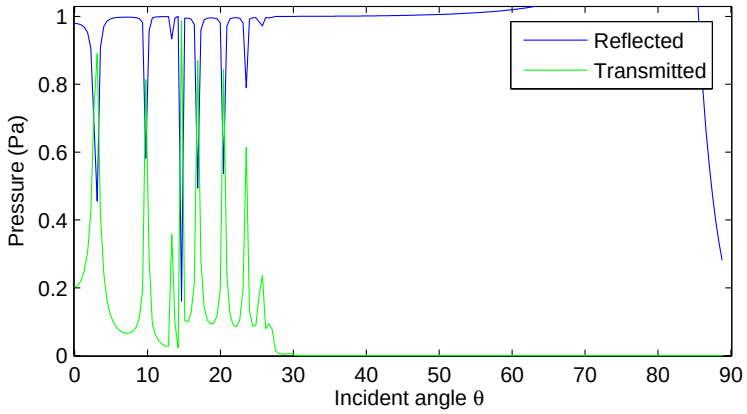

Figure 5.17: Reflected and transmitted pressure through 1.25 cm thick steel plate for y_{HF}

Following this discussion, the pressure distribution and the plate deformation in the y-direction for the incident angles $\theta = 13$ degrees and 19 degrees are plotted in figure 5.18. The incident pressure field is creating a symmetric SW pattern within steel layer, which is similar for both of the incident angles, but the deformation in the y-direction is anti-symmetric for the left plot and symmetric for right plot. This is possibly due to the excitation of different Lamb modes, based on the deformation. It is important to consider the colorbar which indicates the deformation in meters, which demonstrates that there is

very little absolute deformation.

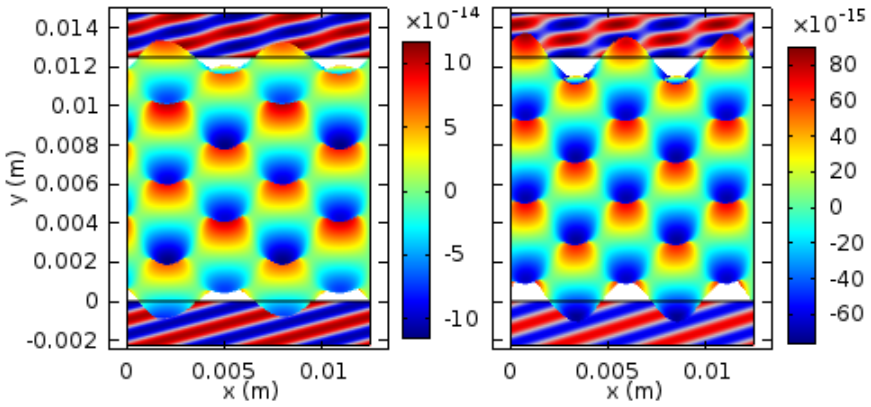

Figure 5.18: Pressure and deformation amplitude in y-direction, with incident angle $\theta = 13$ degrees (left) and 14 degrees (right)

The transmission loss (TL) through the steel plate is presented in figure 5.19 for the HF and the LF wave. In the case of the HF wave there is generally high attenuation, ant the attenuation rises steeply up to 280 dB above an incident angle of 35 degree, which is no transmission. For the LF wave the transmission loss is not nearly as high as for the HF, with almost full transmission at the second resonance angle ($\theta = 37$) degrees. This indicates that in a setting when it is desired to have transmission to the bottom layer, an angle above 37 degrees is not recommended for both cases.

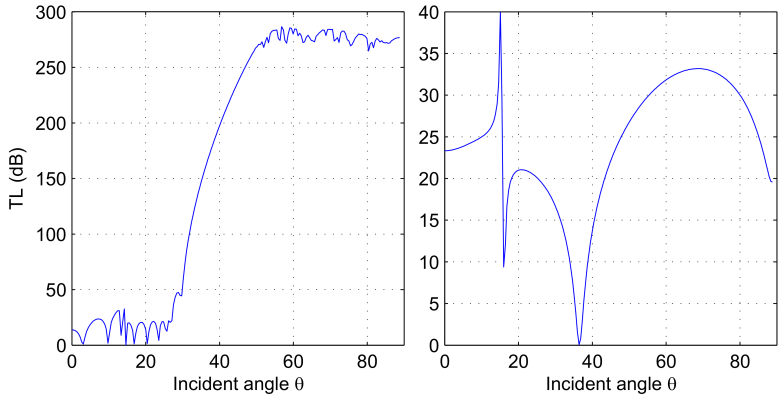

Figure 5.19: Transmission loss as a function of incident angle for HF (left) and LF (right)

5.3.3 Time Domain Study LF

The LF time domain studies with the Acoustic solid interface are performed to investigate how structural wave modes in a steel interface affect the propagation of the acoustic waves in a SURF scheme, and to identify the degree of transmission compared to the frequency domain studies. The studied models are the Acoustic-Solid Interaction and *pitch-catch* models as described in

section 4.5. These models have large dimensions compared to the wavelength, specified in the chapter and steel pipe is simplified to a steel interface. This is to be able to study how a simple transducer model, structural waves and reflection affect the measurements.

The time domain study of the *pulse-echo* model is plotted in figure 5.20 with the pressure distribution over the entire at time $t = 0.025$ ms, 0.07 ms, 0.15 ms and 0.25 ms. Within the solid steel domain, the pressure caused by the structural stress is plotted. In the left most plot in the figure it is observed that the exited pulse can be decomposed into two waves: one high pressure plane wave perpendicular to the transducer surface, and one lower pressure spherical edge wave caused by edge diffraction at the transducer with a pressure ratio of $p_{spher}/p_{plane} = 0.2$. This is a well established principle, both theoretically predicted and observed in practice [25]. While some simplified analysis methods fails to predict the edge wave, FEM shows its strength and accuracy by accurately modeling this phenomenon. As seen at time 0.07 ms the plane waves are dominating, and the main portion of the spherical waves are absorbed at the edges of the model by the plane wave absorbing condition. This is important, since modeling absorbing surfaces in the time domain is difficult, but the plane wave radiation works adequate with the possibility of modeling semi-infinite domains. The deformation of the steel layer causes wave pattern to the edges of the domain at time 0.15 ms. At the last time step ($t = 0.25$ ms.) standing waves have been generated in the bottom layer as earlier discovered in section 4.4.2, while multiple reflections and plate deformation have created an untidy wave pattern in the top layer.

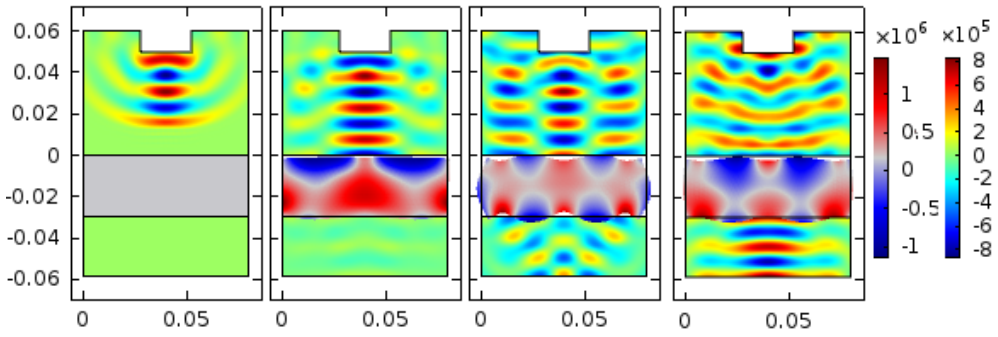

Figure 5.20: Pressure (Pa) distribution from left to right at $t = 0.025, 0.07, 0.15$ and 0.25 ms for normal incident *pulse-echo*

Figure 5.21 illustrates the time response at the transducer and at the bottom, calculated by integration of parametrized curves at the boundaries. The simulated model is described by figure 4.5 for y_{LF}, where the bottom layer is ended with a reflective surface and the layer thickness is $L_2 = 2.985$. The initial pressure at the transducer is the transmitted wave. Due to the long pulse length there is some interference between the initial wave and the reflection observed from 0.06 ms The half-wave resonance is not as well defined as in section 4.4.1, but the build-up of pressure is observable from 0.05 ms and from 0.2 ms the

pressure in the bottom is greater than the reflected pressure. In a SURF study this is favorable, since there will be enough pressure to get substantial time delay to the imaging pulse from the bottom layer.

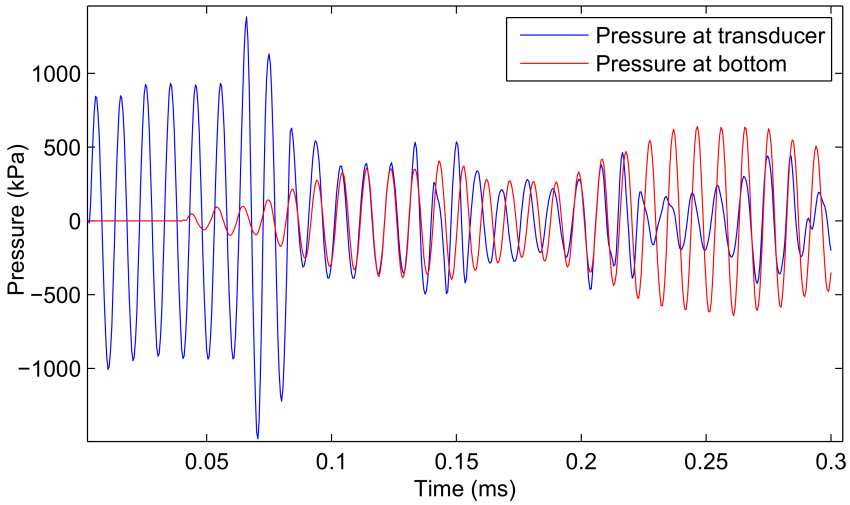

Figure 5.21: Normal incident time series

In figure 5.22, the pressure distribution and plate deformations for the *pitch-catch* model are plotted for the initial time steps $t = 0.02$ ms and 0.04 ms. The receiver is not plotted, since it is only a part of the computations in the post-processing. At the time 0.02 ms the same two-wave composition at the transducer at is figure 5.21 and how the diffracted waves are absorbed at the wall of the domain. In the second time step, a flexural wave in the structural layer has been exited, and interference between the direct and reflected wave is observable. After the initial excitation and reflection, both the wave

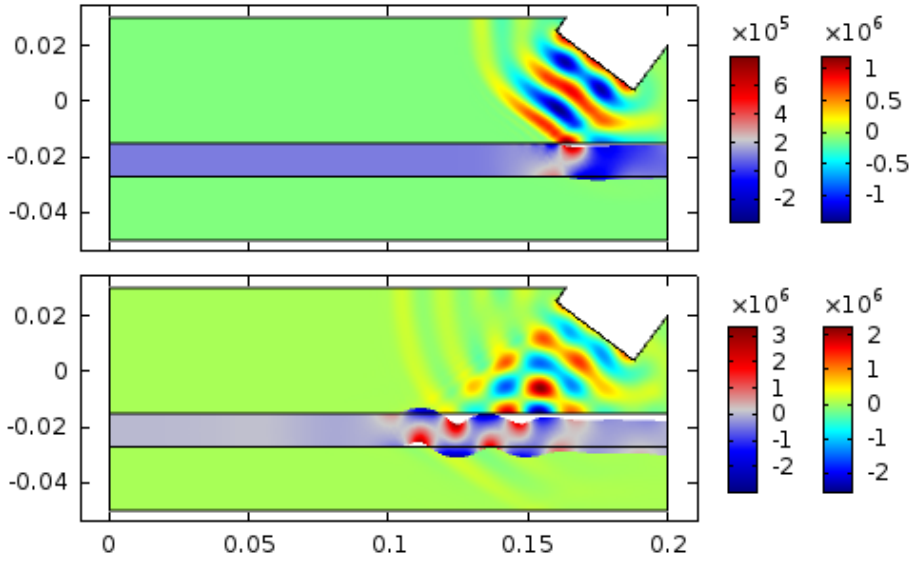

Figure 5.22: Pressure distribution (Pa), internal structural pressure (Pa) and structural deformation at time $t = 0.02$ and 0.04 ms.

in the fluid and in the structural layer continue to propagate in the negative

x-direction, as seen in figure 5.23, at the time steps $t = 0.08$ and 0.13 ms. It is observable how the flexural waves generate pressure waves in the fluid domain as it is evolving in the negative x-direction because the normal particle velocity at the interface between the fluid and structure is conserved. Another consequence of the generation of flexural waves, especially in a dual-frequency SURF analysis, is that flexural waves are dispersive meaning that the speed of sound is frequency dependent and may lead to distortion.

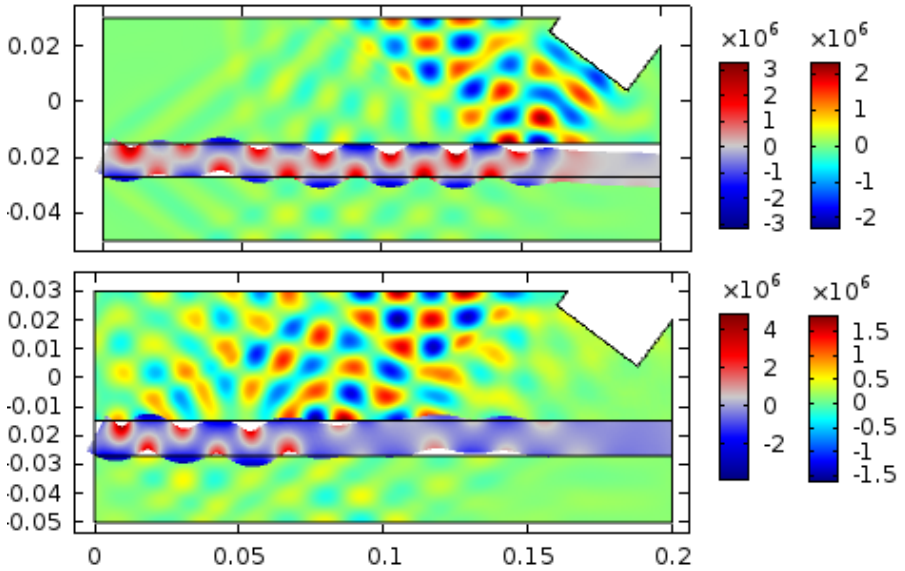

Figure 5.23: Pressure distribution (Pa), internal structural pressure (Pa) and structural deformation at time $t = 0.08$ and 0.13 ms.

The time series at the receiver is plotted in figure 5.24, with source and receiver positioned with a length d apart from each other, and the receiver tilted at the reversed angle of the source. The highest degree of reflection is from the direct reflection from the interface, when the receiver is positioned $d = 2$ cm apart from source making an isosceles triangle with. When the distance is $d = 5$ cm the direct arrival is not visible, a there is interaction between propagating along the surface and reflection for the top boundary. In addition, it is possible to see the low amplitude pressure generated by waves in the solid reaches the receiver ahead in time of the LF pulse at $t = 0.05$ ms. At $d = 0.08$ cm, the main signal is visible from 0.013 ms, and is better defined than for $d = 5$ cm, also the amplitude is greater. Another observation, following the discussion related to figure 5.22 and 5.23, is that it seems clear that structural wave modes have a considerable contribution to the total pressure field. The optimal positioning of the receiver transducer is really dependent on what to study. To study the direct arriving wave the receiver should be placed as the mirror image of the source transducer to make an isosceles triangle. To study reflections from the non-linear layer and flexural waves, the transducer should be placed further away from the transducer where the pressure field is less affected by the direct reflections, from about 0.1 cm in figure 5.23.

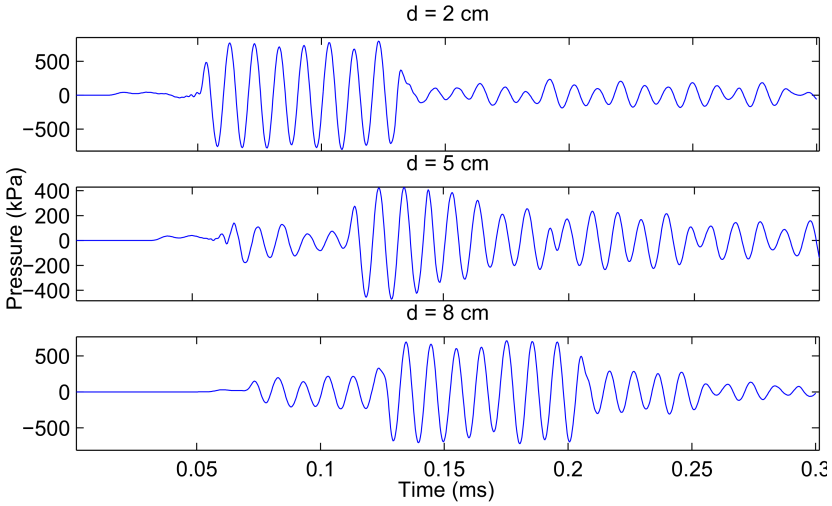

Figure 5.24: Time response at receiver transducer of *pitch-catch* with source and receiver spaced $d = 0.2$ cm , 0.5 cm and 0.8 cm apart

In figure 5.25, the time response below the steel layer with the receiver positioned directly in the path of the direct transmitted wave from the source is plotted. The time response show high attenuation in the solid layer and much reverberation. The frequency domain studies indicated that optimal incident angle was 37 degrees resulting in full transmission, compared to the time domain study there is little transmission at this angle, with a source amplitude of 1 MPa and a transmitted amplitude of 130 kPa it is approximately 10 %. In the situation with the receiver placed in the same layer as the source in a *pitch-catch* study, the low degree of transmission of y_{LF}, may complicate a SURF study. With little modulation pressure in the bottom layer, any effect of SURF will have little influence on the imaging pulse. Another consideration is that any reflections of imaging pulse from the bottom NLL to the receiver will be severely dampened after two transmissions through the steel interface.

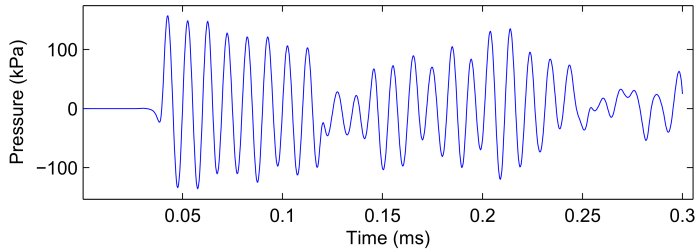

Figure 5.25: Time response below steel interface

The LF time domain simulations with the *Acoustic-Solid Interaction* interface shows the importance of structural wave modes, especially for the *pitch-catch* setup, there is a high degree of interaction between the fluid domain and structural domain.

5.3.4 Time Domain Study HF

Chapter 2.3 described how the degree of convergence of a time dependent FEM study is bounded by the CFL number (time) and the elements per wavelength (geometry). To further complicate the solution, there are two interfaces which are fully coupled, as described in the implementation of the SURF effect in chapter 4.1. In figure 5.26 the total number of degrees of freedom to solve in the *pulse-echo* and *pitch-catch* model as functions of elements per wavelength. The number of degrees of freedom (DOF) are dependent on the shape of the meshing element. In this study a triangular shape is used, and the mesh is constructed by an automatic algorithm with a maximum element size scaled to the HF wavelength. It is observed that the number of DOFs increase rapidly above six elements per wavelength.

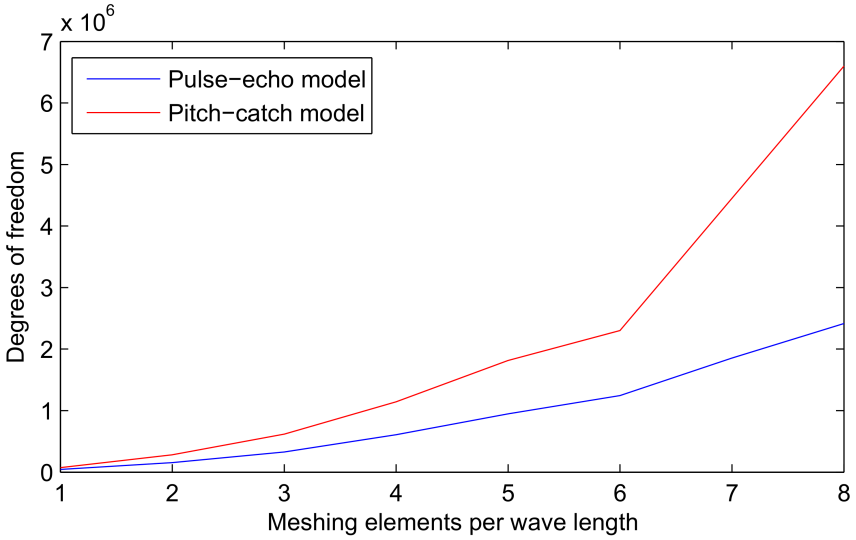

Figure 5.26: Degrees of freedom for the *pulse-echo* and *pitch-catch* models

In a time dependent study the DOF has to be solved for every time step, which generates a long solution time if the time scale of the simulations are long. An example of this is the *pulse-echo* model, which was simulated with the parameters in 5.1 to investigate convergence and solution time.

Table 5.1: Parameters and comp. time for the *pitch-catch* model

Model	EPW	DOF	CFL	Time steps	Comp. time
Pitch-catch	2	260000	0.2	2600	23 hours

When the meshing of the model is scaled to HF pulse and the time scale adjusted to the CLF-condition in (2.34), the solution time is almost one day, and this solution is not converged since there is only two elements per wavelength. By assuming that there is a linear relationship between the degrees of freedom and computational time, it is possible to estimate the computational time for other mesh densities based on this simulation and the computational

time per DOF. Figure 5.27 shows the estimated total computational based on the computational time per DOF. When the minimum six elements condition is satisfied the solution time is almost 200 hours. In addition, it is not unlikely that a higher number is needed due to the complexity of the multiphysical interaction in the acoustic-solid interaction interface, and accordingly a solution time of several weeks is not unlikely. This is a major drawback with the proposed method, and severely complicates the use of the models in a simulation setting with large scales.

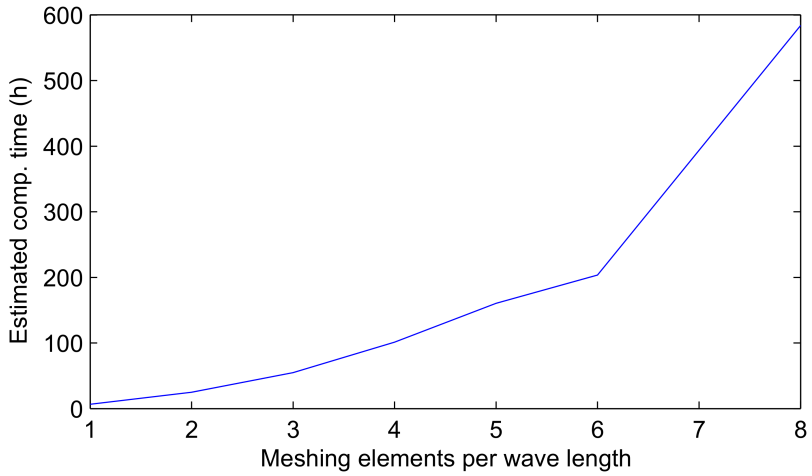

Figure 5.27: Estimated computation time based on DOF for the *pitch-catch* model

Ways to avoid the long computational times is possible. The first way may be to consider other solvers than the direct types, and the applied multifrontal massively sparse direct solver (MUMPS). COMSOL provides numerous different solvers, which all have their strengths, weakness and control parameters, but this is a vast topic within numerical analysis, which further studies are required to find a feasible solution. However, one possibility is to use an iterative solver combined with a multigrid procedure, which is known to be both memory efficient, fast and highly applicable for problems with a high number of DOF [26]. Another solution may be to slightly modify the solution process by initially solving the LF part, store this solution, and afterward solve the HF part segregated by only reading the LF solution and possibly save computational time. There is no obvious way to do this in COMSOL, so this would require more thorough understanding of the possibilities in COMSOL. The simulations will have considerable computational time, regardless of the solver and implementation, because of the limitation in high frequency studies in the FEM method related to the elements per wavelength condition. Based on this discussion on the computational time of the models, the coupled HF and LF SURF implementation is not studied directly and bounded to LF studies in a SURF setting.

6 | Conclusion

The main goal of this thesis was to evaluate the possibility of establishing a simulation tool for the SURF method in the finite element method program COMSOL Multiphysics. The main challenge in the implementation of the SURF method in COMSOL was to introduce a speed of sound dependent of both time and space, as well as the coupling between a low frequency and high frequency solution. The basis of the implementation was the predefined *Pressure Acoustics* interface in COMSOL valid for fluid domains. In chapter 4, the weak-form expression defining the physics in the *Pressure Acoustics* interface was modified to incorporate the time dependent speed of sound in the time derivative by introducing a new variable for the density. By defining two physical interfaces, one linear interface for the low frequency solution and one for the non-linear high frequency solution, the SURF method was implemented by using a fully coupled and simultaneous solution of the two interfaces.

The implementation of the SURF method has been verified to work successfully for several different cases. The SURF implementation was firstly demonstrated on a 2D plane wave channel with a single medium and small dimensions compared to the wavelength. In these simulations, the simulated and theoretical delay caused by the non-linear speed of sound matched with only minor deviations. The model was further implemented with water and steel, both linear and non-linear, and with small geometric dimensions. The results were verified by the identical method as for the plane wave channel, and agreed with the theoretically calculated values. To highlight some of the topics in a SURF scheme and validate the physics, the half and quarter wavelength resonance and standing waves were analyzed considering the modulation pressure caused by the low frequency pulse, time delay and simple SURF processing. It was observed that half wavelength impedance matching and standing waves is an efficient way to ensure transmission through interfaces with large impedance difference, and that it is possible to observe modulation from a non-linear layer behind steel.

The implementation of SURF in the *Acoustic-solid Interaction* interface in COMSOL used the same methodology as for *Pressure Acoustics* interface. This added the possibility to examine the influence of structural wave modes in solids in a SURF study. This SURF implementation was added to a model for normal incident *pulse-echo* and a model *pitch-catch* study of transmission, through a steel pipe simplified to a steel interface. An initial linear frequency

domain study was used to estimate reflection and transmission coefficients as a function of frequency and incident angle. The simulations showed that to ensure transmission, it is incredibly important to consider the incident angle and that wave modes in the structural layer can cause challenges in a real measuring setup, especially for high frequencies. The LF time domain study of the models demonstrated the importance of structural wave modes, and how important the positioning of the receiver transducer in *pitch-catch* studies. Due to the nature of structural waves, the models had to be scaled up to fit a realistic measuring setup, this caused the computational time increase drastically for the HF SURF studies. Convergence study proved that it is not possible to decrease the numerical constraints to the elements per wavelength and time stepping without under sampling the solution. Estimations indicate that a converged solution will have a computation time of several weeks with a direct solver. A further in-depth investigation of the available solvers in COMSOL and the possibility of reducing computational times is necessary to simulate large models. However, the SURF simulation tool is demonstrated to work well for small geometries and is proved to be a versatile way to examine the SURF phenomena.

Bibliography

[1] F.A. Duck. Nonlinear acoustics in diagnostic utrasound. *Ultrasound in Med. and biol.*, Vol. 28(No. 1).

[2] T. Rommetveit, T.F. Johansen, J. Deibele, H. Kaupang, and B. Angelsen. Two way nonlinear manipulation in plane materials using dual frequency pulse complexes. In *Ultrasonics Symposium (IUS), 2010 IEEE*, pages 2380–2383, Oct 2010.

[3] S.-E. Masoy, O. Standal, P. Nasholm, T.F. Johansen, B. Angelsen, and R. Hansen. Surf imaging: In vivo demonstration of an ultrasound contrast agent detection technique. *Ultrasonics, Ferroelectrics and Frequency Control, IEEE Transactions on*, 55(5):1112–1121, May 2008.

[4] T. Rommetveit. *Development of Non-invasive Ultrasound Inspection Techniques through Steel*. PhD thesis, Norwegian University of Science and Technology, Department of Engineering Design and Materials, 2011.

[5] L.E. Kinsler, A.R. Frey, A.B. Coppens, and J.V. Sanders. *Fundamentals of Acoustics*. Wiley, 4th edition, December 1999.

[6] M. Schroeder, T.D. Rossing, F. Dunn, W.M. Hartmann, D.M. Campbell, and N.H. Fletcher. *Springer Handbook of Acoustics*. Springer Publishing Company, Incorporated, 1st ed edition, 2007.

[7] B.A.J. Angelsen. *Ultrasound Imaging - Waves, Signals and Signal Processing Volume 2*. Norway, Emantec, 2000.

[8] J.M. Hovem. *Marine Acoustics- The Physics of Sound in Underwater Enviroments*. USA, Peninsula Publishing, 1st ed edition, 2012.

[9] B.A.J. Angelsen. *Ultrasound Imaging - Waves, Signals and Signal Processing Volume 1*. Norway, Emantec, 2000.

[10] Z.H. Zhu, M.A. Post, and S.A. Meguid. The potential of ultrasonic nondestructive measurement of residual stresses by modal frequency spacing using leaky lamb waves. *Experimental Mechanics*, 52(9):1329–1339, 2012.

[11] F. Tranquart, N. Grenier, V. Eder, and L. Pourcelot. Clinical use of ultrasound tissue harmonic imaging. *Ultrasound in Medicine and Biology*, 25(6):889 – 894, 1999.

[12] T.S. Desser and R.B. Jeffrey. Tissue harmonic imaging techniques: Physical principles and clinical applications. *Seminars in Ultrasound, {CT} and {MRI}*, 22(1):1 – 10, 2001.

[13] Wikipedia. Cross-correlation: Time delay anlysis — Wikipedia, the free encyclopedia. [Online; accessed 31-May-2014].

[14] R.D. Cook, D.S. Malkus, M.E. Plesha, and R.J. Witt. *Concept and Applications of Finite Element analysis*. John Wiley and Sons, Incorporated, 4th ed edition, 2007.

[15] D.E Hutton. *Fundamentals of Finite Element Analysis*. New York, McGraw-Hill, 1st ed edition, 2004.

[16] S. Gagandeep. Short introduction to finite element method. Online NTNU course notes TDT24.

[17] B. Ghose, K. Balasubramaniam, C.V. Krishnamurthy, and A Subhananda Rao. Two dimensional fem simulation of ultrasonic wave. In *Comsol Conference inda*, 2000.

[18] R. Courant, K. Friedrichs, and H. Lewy. Über die partiellen Differenzengleichungen der mathematischen Physik. *Mathematische Annalen*, 100:32–74, 1928.

[19] S.G. Johnson. Notes on perfectly matched layers. Online MIT course notes, March 10 2010.

[20] COMSOL Multiphysics. *COMSOL Acoustics Module User's Guide version 4.3a*.

[21] COMSOL Multiphysics. *COMSOL Multiphysics Reference Guide version 4.4a*.

[22] COMSOL Multiphysics model library. *Acoustic Transmission Loss through Periodic Elastic Structures*.

[23] Z. Su, L. Ye, and Y. Lu. Guided lamb waves for identification of damage in composite structures: A review. *Journal of Sound and Vibration*, 295(3–5):753 – 780, 2006.

[24] S. Santhanam and R. Demirli. Scattering of fundamental lamb wave modes obliquely incident on a surface breaking crack in a plate. In *Ultrasonics Symposium (IUS), 2013 IEEE International*, pages 958–961, July 2013.

[25] Y. Bouzidi and D.R. Schmitt. A large ultrasonic bounded acoustic pulse transducer for acoustic transmission goniometry: Modeling and calibration. *The Journal of the Acoustical Society of America*, 119(1), 2006.

[26] M.F Adams. Multigrid equation solvers for large scale nonlinear finite element simulations. Technical Report UCB/CSD-99-1033, EECS Department, University of California, Berkeley, Jan 1999.

A | Modified Weak Form Expression

The original weak for expression in the *Acoustic-Solid Interaction* interface defining the pressure:

```
(-d(astd.p_t,x)*test(px)-d(astd.p_t,y)*test(py)...
-(d(d(astd.p_t,TIME)-d(astd.p_t,x)*d(x,TIME)...
-d(astd.p_t,y)*d(y,TIME),TIME)-d(d(astd.p_t,TIME)...
-d(astd.p_t,x)*d(x,TIME)-d(astd.p_t,y)*d(y,TIME),x)*d(x,TIME)...
-d(d(astd.p_t,TIME)-d(astd.p_t,x)*d(x,TIME)...
-d(astd.p_t,y)*d(y,TIME),y)*d(y,TIME))...
*test(p)/astd.c^2)/astd.rho
```

The modified SURF weak form expression in the *Acoustic-Solid Interaction interface*. The term rho_user is incorporated into the time derivative, as for *Pressure Acoucstics* interface. This procedure is described in section 4.1.

```
(-d(astd2.p_t,x)*test(p2x)-d(astd2.p_t,y)*test(p2y)...
-(d(d(rho_user,TIME)-d(rho_user,x)*d(x,TIME)...
-d(rho_user,y)*d(y,TIME),TIME)-d(d(rho_user,TIME)...
-d(rho_user,x)*d(x,TIME)-d(rho_user,y)*d(y,TIME),x)*d(x,TIME)
-d(d(rho_user,TIME)-d(rho_user,x)*d(x,TIME)-d(rho_user,y)...
*d(y,TIME),y)*d(y,TIME))...
*test(p2))/astd2.rho
```